Available online at www.sciencedirect.com
ScienceDirect
Geochimica et Cosmochimica Acta 75 (2011) 4899–4916
Geochimica et Cosmochimica Acta
www.elsevier.com/locate/gca

A radiogenic Os component in the oceanic lithosphere? Constraints from Hawaiian pyroxenite xenoliths

Indra Sekhar Sen [a,*], Michael Bizimis [b], Gautam Sen [c], Shichun Huang [d]

[a] Department of Earth & Environment, Florida International University, Miami, FL 33199, USA
[b] Department of Earth and Ocean Sciences, University of South Carolina, Columbia, SC 29208, USA
[c] Office of the Provost, American University of Sharjah, Sharjah, United Arab Emirates
[d] Department of Earth and Planetary Sciences, Harvard University, Cambridge, MA 02138, USA

Received 27 December 2010; accepted in revised form 2 June 2011; available online 14 June 2011

Abstract

Platinum Group Element (PGE) concentrations in garnet pyroxenite xenoliths from Oahu, Hawaii, are significantly lower than those in mantle peridotites and show fractionated patterns (e.g. $Pd_N/Os_N = 2–10$, $Pd_N/Ir_N = 4–24$; N = chondrite normalized) and very high Re_N/Os_N ratios (~9–248). Mass balance calculations show that the bulk rock pyroxenite PGE inventory is controlled by the presence of sulfide phases. The $^{187}Os/^{188}Os$ ratios of these pyroxenites vary from subchondritic to suprachondritic (0.123–0.164); and the $^{187}Os/^{188}Os$ ratios show good correlations with bulk rock and clinopyroxene major and trace element compositions, and bulk rock PGE and sulfur abundances. These observations suggest that the Os isotope compositions in these pyroxenites largely reflect primary processes in the oceanic mantle and Pacific lithosphere.

In contrast, bulk rock $^{187}Os/^{188}Os$ ratios do not correlate with other lithophile isotopic tracers (e.g. Rb–Sr, Sm–Nd, Lu–Hf) which show limited isotopic variability (Bizimis et al., 2005). This and the lack of $^{187}Os/^{188}Os$ vs. Re/Os correlations suggest that the range in Os isotope ratios is not likely the result of mixing between long-lived depleted and enriched components or aging of these pyroxenites within the Pacific lithosphere after its formation at a mid-oceanic ridge setting some 80–100 million years ago. We interpret the Os isotopes, PGE and lithophile element systematics as the result of melt–lithosphere interaction at the base of the Pacific lithosphere. The major and trace element systematics of the clinopyroxenes and bulk rock pyroxenites and the relatively constant lithophile element isotope systematics are best explained by fractional crystallization of a rather homogenous parental magma. We suggest that during melt crystallization and percolation within the lithosphere, the parental pyroxenite melt assimilated radiogenic Os from the grain boundaries of the peridotitic lithosphere. This radiogenic Os component may reside in the grain boundary sulfides or other trace phases, and may be due to fluids or melts that had previously percolated through the basal part of the lithosphere during its transit from a mid-oceanic ridge to its present position above the Hawaiian plume. As the solidus of the parental pyroxenite melt is lower than the solidus of the lithospheric peridotite, we envision that the pyroxenite–parent melt selectively assimilated the grain boundary sulfide phases with lower melting temperature as it percolated through the lithosphere, without significantly reacting with the silicate minerals. Thus while the parental melt of these pyroxenites originate within the Hawaiian plume, melt–lithosphere interaction during progressive crystallization may have selectively enriched the resulting melts with radiogenic Os, thereby decoupling Os from the lithophile element isotopes, but retaining a link between Os, PGE and fractional crystallization systematics. In this model, Oahu pyroxenites essentially represent melts from different stages of this melt–mantle reaction process at the base of the lithosphere, and we suggest that this process may also explain the similar Os vs. lithophile element decoupling seen in the rejuvenated volcanism in Oahu and Kauai. We further show that the pyroxenites do not posses the requisite Pt/Re ratios, where upon, recycling and aging would generate the coupled enrichments of $^{186}Os–^{187}Os$ isotope ratios observed in Hawaiian and other lavas.

* Corresponding author. Present address: Department of Marine Chemistry and Geochemistry, Woods Hole Oceanographic Institution, 360 Woods Hole Rd., Mailstop #25, Woods Hole, MA 02543-1541, USA. Tel.: +1 508 289 3339; fax: +1 508 457 2193.
E-mail address: isen@whoi.edu (I.S. Sen).

0016-7037/$ - see front matter © 2011 Elsevier Ltd. All rights reserved.
doi:10.1016/j.gca.2011.06.008

1. INTRODUCTION

Hawaiian lavas from various eruptive stages (shield, post-shield and rejuvenated) are all conspicuously enriched in their $^{187}Os/^{188}Os$ isotopic compositions. Although there is a general agreement that the enriched Os isotope-signal is a characteristic of the Hawaiian plume (Hauri and Kurz, 1997; Brandon et al., 1998, 1999; Lassiter and Hauri, 1998; Bryce et al., 2005; Ireland et al., 2009), the source of this radiogenic Os remains unclear. Several competing hypotheses have been invoked, such as, input of outer core material (e.g. Brandon et al., 1998) vs. the presence of recycled oceanic crust in the plume (e.g. Lassiter and Hauri, 1998) vs. assimilation of the oceanic crust (e.g. Jamais et al., 2008), and contribution from the in situ Pacific lithosphere (Lassiter et al., 2000).

In this study we take a different approach to understand the extent and origin of radiogenic Os in the oceanic lithosphere. Our approach involves Re–Os isotope and highly siderophile element investigation of the garnet pyroxenite xenoliths from Oahu that appear to have come from the basal part of the Pacific lithosphere (e.g. Sen et al., 2005). These xenoliths are thought to represent high pressure accumulates (>20 kb) from melts similar to their host rejuvenated stage Honolulu Volcanics series lavas (HV) (Sen, 1983, 1988; Bizimis et al., 2005; Keshav et al., 2007). Because these xenoliths reside in the deeper part of the oceanic lithosphere, it is likely that their chemical compositions were not obscured by subsequent low pressure crystallization/assimilation processes en route to the surface that may have affected the composition of the erupted lavas. We show that the enriched Os signature may not have a plume origin but instead is a product of magma–lithosphere reaction process, where the pyroxenite–parent melts selectively assimilated radiogenic Os from the grain boundary sulfide phases while percolating through the Pacific lithosphere.

2. GARNET PYROXENITE XENOLITHS

There is a significant body of published information on petrography, mineral chemistry, trace element and isotope geochemistry of the Salt Lake Crater (SLC) pyroxenite xenoliths (Green, 1966; White, 1966; Jackson and Wright, 1970; Frey, 1980; Sen, 1988; Keshav and Sen, 2001; Bizimis et al., 2005; Sen et al., 2005, 2010; Keshav et al., 2007). Thermobarometry, the Sr–Nd–Hf isotope compositions and trace element systematics of the xenoliths, suggest that the pyroxenites are near zero-age high pressure (>20 kb) cumulates from melts similar to the rejuvenated Hawaiian volcanism and the HV lava series (Sen, 1983; Bizimis et al., 2005; Sen et al., 2005; Keshav et al., 2007). The presence of garnets with majoritic precursors (Keshav and Sen, 2001) and nano-diamonds (Wirth and Rocholl, 2003) in some rare xenoliths suggest that at least a few of these pyroxenites were brought up from a depth of 180–270 km ($P = 60$–90 kb) by the Hawaiian plume. The general consensus is that, with the exception of a few of these deep upper mantle fragments, the bulk of these pyroxenites formed as igneous veins near the base of the lithosphere.

Lassiter et al. (2000) reported the first bulk rock $^{187}Os/^{188}Os$ isotope data on six pyroxenite xenoliths from the Salt Lake Crater (Oahu, Hawaii) and found them to be relatively radiogenic in $^{187}Os/^{188}Os$ (0.134–0.175), but at unradiogenic and constant $^{87}Sr/^{86}Sr$ ratios (0.7032–0.7033). In their model, the radiogenic Os results from the ingrowth of ^{187}Os from ^{187}Re, while the pyroxenites remained stored in the Pacific lithosphere for 80–100 Myr, the approximate age of the ocean floor beneath Oahu. Lassiter et al. (2000) suggested that the xenoliths represent 80–100 Myr old cumulates at the base of the lithosphere, that were once formed at a paleo mid-ocean ridge setting.

Thus a discrepancy exists between the radiogenic Os isotope signatures in the SLC pyroxenites, that require a relatively long-lived Re/Os fractionation and the zero-age depleted isotope signatures from the Hf–Nd–Sr isotope systematics. The samples analyzed here for Os isotope and PGE contents are the same ones that were previously reported by Bizimis et al. (2005), which allow us to compare the Os and Hf–Nd–Sr isotope systematics of the SLC pyroxenites on the same sample and explore their petrogenesis in the multi-isotope and element space.

3. ANALYTICAL TECHNIQUES

The samples studied here are from Dean Presnall Collection, now housed at the Smithsonian Institution. The samples range from garnet pyroxenites to websterites. For bulk rock trace element, S, HSE and Os isotope analyses, the samples were coarsely crushed to expose the interior fragments of the xenoliths. Interior pieces were handpicked to avoid obvious surface alterations or voids, and powdered either by hand grinding with a pre-cleaned and preconditioned ceramic alumina mortar and pestle, or agate bowl.

Bulk rock trace elements were determined on a Thermo Scientific ELEMENT2-High Resolution ICP-MS at the Center for Element Mass Spectrometry, Department of Earth and Ocean Sciences, University of South Carolina. Briefly, about 50 mg of sample powder was digested in 4 ml of Teflon-distilled HF:HNO_3 (3:1 mixture) at 100 °C for 48 h. After digestion the samples were dried and redissolved in concentrated 1 ml HNO_3 (two times). Trace element concentrations were determined at 100 ppm total dissolved solid solutions and spiked with In as an internal standard. Each sample was analyzed in duplicate. Full processing blanks were measured and corrected for every acquisition sequence. We used BHVO-2 as an external standard and the BIR-1 standard was analyzed as an unknown (Jochum and Nehring, 2006; Jochum et al., 2006). The pyroxenite bulk rock trace element data along with the BIR-1 and BHVO-2 values used for calibration are reported in Table 1.

Bulk rock sulfur was determined at Activation Laboratories Limited, Canada on a Leco CNS 2000. Sulfur is measured as SO_2 produced by the combustion of 0.2 g rock powder and the data is reported in Table 1. For the quality control of the data USGS certified standard Green River Shale (SGR-1) was analyzed as an unknown. The measured S concentration of SGR-1 (1.5%) agrees well with the USGS certified value (1.53 wt%).

Table 1
Bulk rock trace element (μg/g) and sulfur concentrations.

Sample no.	552	553	555	559	714	716	744	590	594	620	571	776	BIR -1 measured	BIR-1 reported	BHVO-2 standard used
Rock type	gp	gp	gp	gp	gp	gp	gp	o	o	o	w	w			
Cpx (mode)	95%	85%	80%	85%	80%	95%	60%	80%	85%	75%	75%	50%			
Mg# Cpx	0.69	0.76	0.77	0.77	0.75	0.8	0.68	0.78	0.78	0.80	0.84	0.84			
Al_2O_3 Cpx	7.29%	5.96%	6.87%	7.39%	6.34%	5.69%	7.40%	6.70%	6.51%	6.52%	5.06%	6.03%			
Gt (mode)	5%	5%	20%	15%	20%	3%	40%	15%	10%	20%	5%				
Mg# Gt	0.62	0.61	0.68	0.65	0.63	0.7	0.62	0.67	0.69	0.68	0.75				
Opx (mode)		10%				5%		2%	5%	5%	20%	50%			
Mg# Opx		0.78				0.78		0.79	0.79	0.81	0.84	0.84			
Cs	0.05	0.01	0.005	0.06	0.01	0.02	0.003	0.004	0.01	0.01	0.01	0.01	0.01	0.01	0.10
Rb	13.17	0.96	0.80	3.86	1.47	1.18	0.95	1.02	0.62	1.92	0.58	0.38	0.20	0.20	9.11
Ba	273	76	15	134	47	133	47	58	35	64	15	5	6	7	131
Th	0.22	0.26	0.20	0.23	0.09	0.08	0.12	0.11	0.15	0.28	0.09	0.08	0.03	0.03	1.22
U	0.09	0.07	0.06	0.09	0.04	0.03	0.04	0.04	0.05	0.16	0.02	0.02	0.01	0.01	0.40
Nb	5.43	2.61	1.01	1.99	0.86	0.81	0.84	0.45	0.77	1.85	0.62	0.91	0.51	0.55	18.10
Ta	0.43	0.18	0.13	0.11	0.09	0.08	0.10	0.10	0.06	0.19	0.06	0.06	0.04	0.04	1.14
La	2.86	3.16	2.39	3.33	1.60	1.99	1.81	1.90	1.86	3.19	1.29	1.08	0.67	0.62	15.20
Ce	8.1	7.0	6.5	7.5	4.7	4.0	5.8	6.1	4.7	8.5	3.5	3.1	2.0	1.9	37.5
Pb	0.47	0.42	0.16	0.50	0.29	0.12	0.08	0.62	0.28	0.47	0.18	0.25	2.54	3.10	1.70
Pr	1.36	1.02	1.07	1.26	0.80	0.70	1.04	1.04	0.75	1.23	0.60	0.49	0.37	0.37	5.35
Sr	690	225	140	239	90	472	85	104	63	128	53	38	107	109	396
Nd	7.54	5.03	5.65	6.61	4.32	3.93	6.04	5.37	3.96	5.99	3.40	2.56	2.37	2.38	24.50
Zr	61	31	32	24	26	20	47	23	15	26	11	13	14	14	172
Hf	2.43	1.02	1.08	1.03	1.11	0.77	1.83	0.73	0.67	0.85	0.55	0.48	0.58	0.58	4.36
Sm	2.69	1.63	1.77	2.22	1.53	1.41	2.23	1.62	1.30	1.79	1.23	0.85	1.08	1.12	6.07
Eu	1.09	0.63	0.65	0.85	0.59	0.58	0.87	0.60	0.48	0.67	0.45	0.31	0.51	0.53	2.07
Ti	16,315	4006	4815	4723	6315	3990	6406	3164	3398	3613	2967	2395	5159	5600	16,300
Gd	3.62	2.10	2.00	2.69	1.65	1.86	2.82	1.80	1.63	2.10	1.44	1.01	1.78	1.87	6.24
Tb	0.53	0.33	0.29	0.43	0.28	0.30	0.45	0.27	0.23	0.35	0.23	0.16	0.33	0.36	0.92
Dy	3.16	2.14	1.66	2.58	1.63	1.86	2.75	1.53	1.42	2.20	1.37	0.95	2.54	2.51	5.31
Ho	0.55	0.41	0.29	0.48	0.29	0.36	0.51	0.28	0.25	0.41	0.24	0.17	0.56	0.56	0.98
Y	14.13	10.68	7.48	12.39	7.18	9.57	13.19	7.09	6.45	10.86	6.24	4.50	15.33	15.60	26.00
Er	1.29	1.11	0.72	1.20	0.70	0.93	1.30	0.69	0.62	1.07	0.60	0.45	1.69	1.66	2.54
Yb	0.93	0.91	0.52	0.90	0.48	0.70	1.02	0.53	0.45	0.82	0.42	0.36	1.62	1.65	2.00
Lu	0.13	0.13	0.07	0.12	0.06	0.10	0.14	0.07	0.06	0.11	0.05	0.05	0.24	0.25	0.27
Sc	20.98	32.60	29.41	27.69	21.68	27.36	21.46	26.96	26.09	30.26	30.61	20.17	41.64	43.00	32.00
V	390	280	316	297	305	262	283	215	247	269	243	166	307	319	317
Cr	444	1072	907	912	991	1101	305	2312	1742	1448	2337	2349	364	391	280
Co	70	62	60	59	71	57	79	61	58	61	51	51	50	52	45
Ni	341	434	489	474	502	486	490	712	616	636	566	573	160	166	119
Cu	74	127	63	153	78	91	101	74	112	98	45	45	115	119	127
Zn	26	37	38	25	48	34	33	43	24	36	21	24	41	72	103
Ga	18	13	14	13	16	12	15	10	10	15	9	7	15	15	22
Cd	0.04	0.04	0.04	0.04	0.03	0.03	0.04	0.04	0.03	0.03	0.03	0.02	0.03	0.10	0.06
Sn	1.23	0.35	0.47	0.62	0.66	0.36	1.14	0.52	0.35	0.41	0.28	1.49	0.67	0.60	1.70
Sulfur (wt%)	0.188	0.028	0.117	0.118	0.117	0.009	0.281	0.102	0.06	0.054	0.04	0.044			
Sulfide (mode)	0.51%	0.08%	0.32%	0.32%	0.32%	0.02%	0.76%	0.28%	0.16%	0.15%	0.11%	0.12%			

Note: Mg# = Mg/(Mg + Fe) and Al_2O_3 data from Bizimis et al. (2005) and SL-594 from Sen et al. (2010).
gp, garnet pyroxenite; o, olivine bearing garnet pyroxenite; w, websterite.
All samples have the prefix of 77SL-.

Bulk rock HSE and Os isotopes were determined at the Geochemistry Division, National High Magnetic Field Laboratory, Florida State University with the "carius-tube" digestion technique, following the method of Puchtel et al. (2004a). About 2.5 g of sample powder were spiked with an isotopically enriched PGE solution (spike #000601, provided by Prof. Munir Humayun, FSU, enriched in the following isotopes: ^{99}Ru, ^{110}Pd, ^{185}Re, ^{190}Os, ^{191}Ir, ^{195}Pt). The spiked powders were digested with ~10 ml "inverse Aqua Regia" (3:1 HNO_3:HCl) in pre-cleaned borosilicate glass tubes at 240 °C for 72 h. After digestion, the tubes were thoroughly chilled in ice to prevent possible Os volatilization during opening. Osmium was extracted first from the aqua regia solution using carbon tetrachloride (CCl_4)

solvent extraction technique, then back-extracted to HBr and finally purified via micro distillation using chromic acid as an oxidizer and collected in a drop of HBr (Birck et al., 1997). The Ir–Pt–Pd–Ru fraction was extracted from one half fraction of the extracted aqua regia by cation exchange chromatography using 10 ml of AG50W-X8 exchange resin in 0.15 N HCl (Puchtel et al., 2005). The samples were passed twice through the columns to ensure a clean PGE fraction and minimize potential isobaric interferences. Rhenium was extracted from the remaining aqua regia solution by anion exchange chromatography in weak HNO_3, following the techniques outlined in Lassiter (2003). Extra care was taken to carefully and slowly dry down the fractions containing Re in order to avoid possible loss of Re because of volatilization.

The Ir, Pt, Pd, Ru concentrations were determined on a FinniganMat ELEMENT-1-HR-ICP-MS using an MCN-6000 desolvating nebulizer (CETAC) coupled with (50 µl) PFA nebulizer (ESI) in 0.15 N HCl matrix. We used the ratios: $^{193}Ir/^{191}Ir$, $^{198}Pt/^{195}Pt$, $^{99}Ru/^{102}Ru$, $^{105}Pd/^{110}Pd$, so as to minimize isobaric interferences for other elements (e.g. Mo on Ru) or species. In addition, the instrument was tuned for low oxide formation as to suppress potential oxide interferences, e.g. $^{94}Zr^{16}O$ on ^{110}Pd; ZrO+/Zr+ < 0.03%. We also monitored potential interferences from ^{110}Cd on ^{110}Pd and ^{198}Hg on ^{198}Pt by monitoring ^{111}Cd, ^{112}Cd, ^{113}Cd and ^{199}Hg, ^{200}Hg, respectively. In no case any of these corrections amounted to more than 2% of the signals. Mass fractionation was corrected using the linear law against an in-house 1 ng/g mixed Re–PGE standard. Instrument background was determined on the wash acid at the same normality as the samples, and subtracted from the isotope-signals prior to fractionation correction. Total procedural blanks are reported in Table 2.

Some Re analyses were also performed on the ELEMENT-1 using an MCN-6000 desolvating nebulizer coupled with a 50 µl PFA nebulizer, while others were performed on a Neptune® MC-ICP-MS, and in both cases using a sample-standard bracketing method. An in-house Re standard, made from Re wire, was used to correct the instrumental isotopic fractionation. The $^{187}Re/^{185}Re$ ratio of this in-house Re standard was determined independently using a W-doping method. Specifically, this in-house Re standard solution was mixed with NIST SRM 3163 W standard solution, and was then introduced into Neptune via an APEX nebulizer. Peaks of ^{182}W, ^{183}W, ^{184}W, ^{185}Re, ^{186}W, ^{187}Re and ^{190}Os were monitored. Instrumental fractionation was corrected to $^{186}W/^{184}W = 0.927633$ (Völkening et al., 1991), and ^{187}Os interference on ^{187}Re, if any, was corrected online using $^{187}Os/^{190}Os = 0.06$. Fourteen repeat measurements of this in-house Re standard give an $^{187}Re/^{185}Re$ average of 1.66909 ± 0.00005 (2 SD), which is ~0.3 per mil lighter than most commercially available Re standard solutions (Hu et al., 2011).

Os isotope ratios were determined on the Neptune® MC-ICP-MS. After microdistillation, the HBr drop containing the purified Os was diluted with 18 MΩ H_2O to make 0.1 ml 2% HBr solution, and introduced to Neptune® MC-ICP-MS using an APEX® coupled with a 40 µl/min nebulizer. Peaks of ^{185}Re, ^{187}Os, ^{188}Os, ^{189}Os, ^{190}Os and ^{192}Os are monitored, and instrumental mass fractionation is corrected to $^{192}Os/^{188}Os = 3.083$ using an exponential law. The integration time is 8 s, and 10–15 ratios can be obtained with 0.1 ml solution. A 20 ng/g in-house Os standard, MixA, was repeatedly measured during the course of analysis in order to monitor the external reproducibility of Os isotopic measurement. One typical measurement of 20 ng/g MixA standard yielded a ^{188}Os signal of ~100 mV, and contained 15 ratios, which consumed ~1 ng Os. The average $^{187}Os/^{188}Os$ of MixA is 0.1268 ± 0.0007 (2σ, $n = 20$). The total procedural Os blank averaged 2.7 pg ($n = 4$; Table 2). The HSE and Os isotope ratios of the bulk rocks are reported in Table 2. Because of their low Os signals (^{188}Os 4–70 mV) the sample Os isotope ratios were analyzed in a transient mode as follows: acquisition begun while the sample was in the wash solution (0.1 N HBr). Twenty ratios of the background were collected and then the probe was moved into the sample vial. Once the signal stabilized we acquired 13–15 ratios before the solution was exhausted. The isotope compositions were determined offline and the wash intensities determined before each sample were used to correct each isotope's intensity for background. The difference between the background (wash) $^{187}Os/^{188}Os$ corrected ratios and the uncorrected ratios were from 0.1% to 5% for the samples with the smallest Os signals (samples SL-744 and SL-716), and scales almost linearly with the 2σ error of the $^{187}Os/^{188}Os$ ratio for each sample, which is also a function of signal intensity. The Re signals where always near background and correction of the ^{187}Re on ^{187}Os resulted in <0.5% correction on the $^{187}Os/^{188}Os$ ratios of the samples. There was no correlation between isotope ratios and Os signal intensities, or Os concentrations in these samples (discussed later). Compared to the total ~28% $^{187}Os/^{188}Os$ ratio variability seen within our sample population, the corrections applied to the $^{187}Os/^{188}Os$ ratios are relatively minor.

4. RESULTS

4.1. Bulk rock lithophile trace element characteristics

Primitive mantle normalized trace element concentrations of the pyroxenites are plotted in Fig. 1. The figure also shows a comparison with the concentrations of clinopyroxene and garnet separates from these samples (Bizimis et al., 2005). It is apparent that, with the exception of the highly incompatible elements Cs, Rb, Ba and occasionally Sr, all elemental abundances in the bulk rock can be broadly explained as a mixture of garnet and clinopyroxene. While we cannot be absolutely certain, the higher values for Cs, Ba, Rb and Sr are consistent with trace amounts of amphibole and phlogopite that sometimes occur in these rocks (Sen, 1983, 1987, 1988; see also Table 3).

The highly incompatible element (Cs, Rb, Ba, U, Th, Nb, Sr, Ta, La and Ce) concentrations in the bulk rock do not correlate with Mg# or Al_2O_3 content of clinopyroxenes (Bizimis et al., 2005). In contrast, the REE and compatible element (Ni, Cr) concentrations in the pyroxenites generally correlate well with Mg# and Al_2O_3 content of

Table 2
Bulk rock HSE concentrations (ng/g) and Os isotope ratios.

Sample no.	HSE in bulk rock										
	Os	Ir	Ru	Pt	Pd	Re	Pd/Ir	Re/Os	Pt/Re	$^{187}Os/^{188}Os$	2σ[a]
552	0.24	0.12	0.45	1.72	2.75	1.12	23.8	4.7	1.54	0.1643	7
555	0.08	0.05	0.08	0.68	0.35	1.71	7.7	20.2	0.40	0.1464	7
559	0.48	0.35	1.37	3.22	3.51	0.91	10.0	1.9	3.55	0.1556	6
714	0.14	0.09	0.63	0.69	0.82	1.05	8.8	7.6	0.66	0.1334	9
716	0.03	0.04	0.14	10.44	0.15	0.18	3.6	5.5	58.57	0.1361	36
744	0.21	0.09	0.20	1.04	1.29	1.59	15.0	7.5	0.65	0.1535	51
590	0.95	0.62	1.19	3.85	2.41	1.03	3.9	1.1	3.73	0.1362	1
594	0.68	0.43	1.21	3.43	4.20	1.21	9.7	1.8	2.85	0.1540	12
620	0.52	0.35	0.74	2.16	1.27	0.95	3.6	1.8	2.29	0.1401	21
571	0.09	0.07	0.26	7.61	0.28	0.62	4.3	6.6	12.29	0.1233	8
776	0.66	0.42	0.99	2.87	3.44	0.48	8.3	0.7	5.92	0.1324	2
Blank ($n = 4$)	2.7 pg	2 pg	5 pg	226 pg	10 pg	7 pg					

All sample have the prefix of 77SL-.
[a]Errors on measurements are uncertainty on the last significant digit for Os.

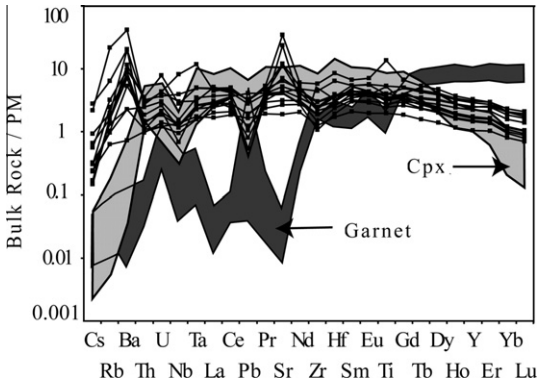

Fig. 1. Primitive mantle normalized trace element concentrations in the bulk rock compared with concentrations in clinopyroxene and garnet (Bizimis et al., 2005). Primitive mantle normalization values from McDonough and Sun (1995).

the clinopyroxenes where the most Ni and Cr enriched samples have the highest Mg# and lowest REE and Al_2O_3 concentrations (Fig. 2).

4.2. HSE and sulfur systematics

The HSE concentrations in the studied pyroxenites are 10–100 times depleted compared to the primitive upper mantle composition (Becker et al., 2006). The absolute HSE concentrations show more than one order of magnitude variability with relatively higher HSE concentrations in the websterites relative to the pyroxenites (Fig. 3a). The concentration ranges for the Hawaiian pyroxenites are similar to pyroxenite data from other localities (Kumar et al., 1996; Pearson and Nowell, 2004; Luguet et al., 2008; Van Acken et al., 2010). The SLC garnet pyroxenites and websterites are enriched in Pd, Pt and Re relative to Os, Ir and Ru and show strongly fractionated PGE patterns ($Pd_N/Os_N = 2–10$, $Pd_N/Ir_N = 4–24$; N = chondrite normalized) and high Re_N/Os_N ratios (~9–248). The individual PGE show good positive correlations with each other (Fig. 4), for example, good correlations exist between Os, Ir, Ru ($R^2 > 0.9$) and moderate correlation between Os and Pd ($R^2 = 0.6$). Platinum shows a strong positive trend with Ir, Os and Ru, however there are two samples (SL-571; SL-716) that have anomalously high Pt contents (Fig. 4b). Similar platinum enrichments have also been observed in peridotite xenoliths (Ackerman et al., 2009), basalts (Bennett et al., 2000) and pyroxenites (Maier et al., 2001; Luguet et al., 2008) and occasionally in sulfides within these pyroxenites (Sen et al., 2010), and maybe related to Pt-nugget effects. Unlike the other siderophile elements, Re is decoupled from the PGEs (Fig. 4e).

The absolute abundances of PGEs do not correlate with Mg# or Al_2O_3 content of the clinopyroxenes. Incompatible/compatible PGE ratios such as Pd/Os, Pd/Ir, Pd/Ru show good intra-correlations (not shown, Pd/Ir vs. Pd/Os,

Table 3A
Sulfide mode calculation.

Sample no.	Phases	Bulk rock	Clinopyroxene	Phlogopite	Garnet	Sulfide
SL-552	(Ni) ppm	341	139	820	30	47,000
	Mode		94%	1%	5%	0.42%[a]
SL-744	(Ni) ppm	490	169	0	23.4	51,400
	Mode		60%	0%	40%	0.74%[a]
SL-559	(Ni) ppm	473.5	201	0	30	58,900
	Mode		85%	0%	15%	0.51%[a]

[a] Modal abundance of sulfide obtained by mass balancing Ni between bulk rock and its constituent phases.

Table 3B
Mass balance for HSE.

Sample no.	Phase	Os	Ir	Pt	Pd	Re
SL-552	Sulfide (average ± 1σ SD, μg/g)	0.13 ± 0.1	0.07 ± 0.06	0.22 ± 0.16	0.35 ± 0.26	0.22 ± 0.08
SL-744	Sulfide (average ± 1σ SD, μg/g)	0.03 ± 0.02	0.02 ± 0.01	0.07 ± 0.04	0.14 ± 0.05	0.23 ± 0.12
SL-559	Sulfide (average ± 1σ SD, μg/g)	0.33 ± 0.23	0.32 ± 0.29	0.08 ± 0.06	0.2 ± 0.12	0.42 ± 0.02
SL-552	Bulk calculated (ng/g)	0.54 ± 0.4	0.31 ± 0.23	0.94 ± 0.69	1.47 ± 1.1	0.91 ± 0.06
	Bulk measured (ng/g)	0.24	0.12	1.72	2.75	1.12
SL-744	Bulk calculated (ng/g)	0.24 ± 0.15	0.14 ± 0.1	0.55 ± 0.27	1.03 ± 0.34	1.73 ± 0.88
	Bulk measured (ng/g)	0.21	0.09	1.04	1.29	1.59
SL-559	Bulk calculated (ng/g)	1.69 ± 1.16	1.63 ± 1.47	0.39 ± 0.31	1.02 ± 0.6	2.12 ± 0.08
	Bulk measured (ng/g)	0.48	0.35	3.22	3.51	0.91

Ni content in mineral phases from Bizimis et al. (2005); BR, bulk rock; SD, standard deviation.
Major and PGE concentrations for sulfides are from Sen et al. (2010).

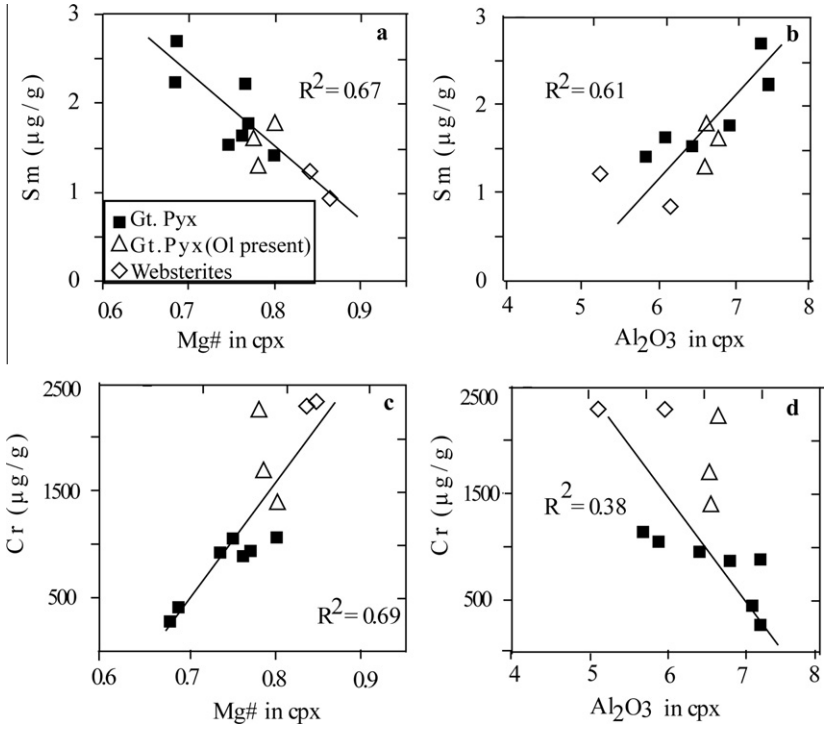

Fig. 2. Mg number (molar $Mg/Mg + Fe_{Total}$) and Al_2O_3 content in clinopyroxene vs. Sm and Cr content of the bulk rock. Clinopyroxene data from Bizimis et al. (2005).

$R^2 \sim 0.6$; Pd/Ir vs. Pd/Ru, $R^2 \sim 0.72$), however the ratios do not correlate with major and trace element concentrations of clinopyroxenes and bulk rock.

The analyzed xenoliths show a large range of S concentrations (0.01–0.28 wt%, Table 1). The S contents correlate with major and trace element and isotope compositions of the bulk rock and the clinopyroxenes: the most S enriched samples have the highest Pd/Ir, Al_2O_3, $^{187}Os/^{188}Os$ and lowest Mg# (Fig. 5). This correlations suggest that the S contents reflect a primary mantle process and by inference a systematic sulfide incorporation process. However, there is no correlation between bulk S and PGE contents (Fig. 5e and f), consistent with the lack of correlation between PGE contents and major or lithophile trace elements. Furthermore, the lack of correlation between bulk rock sulfur contents and absolute bulk rock PGE abundances (Fig. 5e and f) is consistent with the variable (two orders of magnitude) PGE contents in the sulfides in these pyroxenites (Sen et al., 2010).

4.3. Sulfide controls the PGE budget of the pyroxenites

Based on the bulk rock S concentrations and assuming that silicate phases contain 0 wt% sulfur, we calculate that the SLC pyroxenites have 0.02–0.76 wt% modal sulfide abundance. The sulfides in these pyroxenites have been previously interpreted as immiscible liquid separated from a silicate melt that crystallized the garnet and the clinopyroxenes (Sen et al., 2010). As the sulfide/silicate partition coefficients are very high for the HSE (e.g. >10,000; Crocket

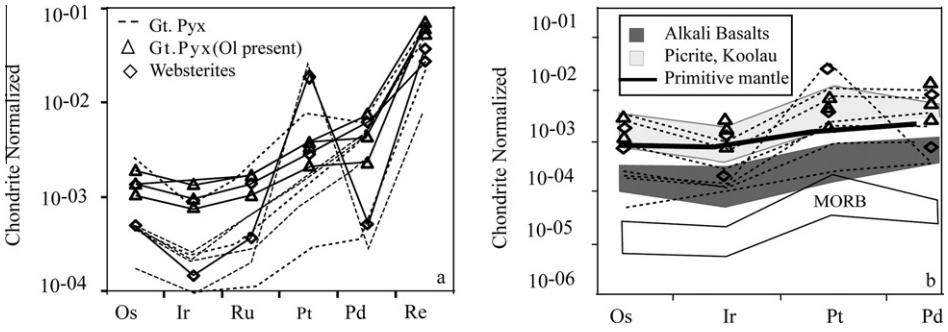

Fig. 3. (a) Chondrite normalized PGE pattern of garnet pyroxenites ± olivine and websterites. (b) Pyroxenites data compared to published PGE data: dark gray area, alkali basalts from Maui, Hawaii (Crocket, 2002); light gray area, picritic lavas from Koolau, Hawaii (Ireland et al., 2009); Pacific MORB field is based on the data reported by Schiano et al. (1997) and Tatsumi et al. (1999); solid bold line presents primitive mantle model composition after Becker et al. (2006). The garnet pyroxenites and the websterites have similar chondrite normalized PGE pattern with enrichments in Pt and Pd over Os and Ir. In general, relative to the Pacific MORB, the pyroxenites have higher PGE concentrations. CI normalized values from McDonough and Sun (1995).

et al., 1997; Fleet et al., 1999; Sattari et al., 2002), it is reasonable to assume that sulfides may be the major repository of HSEs in the pyroxenites, as has been demonstrated for peridotites (e.g. Alard et al., 2000; Lorand and Alard, 2001). However, the relation of sulfides to the PGE budget of pyroxenites at upper mantle conditions has never been explicitly investigated.

In an effort to investigate to what degree sulfides control the PGE and Re budget in the bulk rock pyroxenite, we carried out detailed mass balance calculations on three pyroxenites (samples SL-552, SL-744 and SL-559), for which, both sulfide (Sen et al., 2010) and bulk rock PGE data exist (this study). In order to have an additional check on the sulfide modal abundance (calculated from the S measurements), we also performed rigorous Ni mass balance calculations between the constituent phases and the bulk rock on the same pyroxenites, based on the measured Ni contents of the silicates, sulfides, and bulk rock. Using the appropriate mineral modes and Ni concentrations in the bulk rock and the other silicate phases, we calculated 0.42–0.74 wt% of sulfide mode (Table 3A), which is very similar to the estimate from the S measurements for these samples (Table 1).

We then use this modal abundance to calculate bulk rock PGE and Re concentrations using the average PGE concentrations in the sulfides from the corresponding rocks (Sen et al., 2010), and assuming no PGE or Re in the silicate phases. The calculated bulk rock Os, Ir and Re concentrations overlap (within error) with the measured values (Table 3B and Fig. 6a–c), while Pd and Pt concentrations fall close to but generally higher than the measured values. We note that the in situ PGE sulfide data (Sen et al., 2010) used here for the mass balance was necessarily restricted to large sulfide grains (>50 μm). It is conceivable that smaller Pd and Pt enriched sulfide grains exist that are not easily identified during routine petrographic work but nonetheless contribute to the PGE budget of the bulk rock. In general, our investigation shows that sulfides are indeed the major host of PGE and Re in pyroxenitic lithologies (bearing the occasional presence of minor Pt–Pd enriched phases) and the Re–PGE systematics of these sulfides are largely reflected in the bulk rock chemistry.

4.4. Osmium isotope systematics

The osmium isotope data of the SCL pyroxenites are reported in Table 2. The $^{187}Os/^{188}Os$ ratios vary from subchondritic to suprachondritic (0.1233–0.1643). Our new data overlap and extend to less radiogenic $^{187}Os/^{188}Os$ ratios than the dataset of Lassiter et al. (2000), and largely overlap the Os isotope range of Hawaiian lavas in general (Hauri and Kurz, 1997; Brandon et al., 1998, 1999; Lassiter and Hauri, 1998; Lassiter et al., 2000; Jamais et al., 2008; Ireland et al., 2009). We note that the websterites have relatively unradiogenic Os (0.1233–0.1324) when compared to garnet pyroxenites (0.1334–0.1643) and the $^{187}Os/^{188}Os$ ratios do not correlate with $^{187}Re/^{188}Os$ (Fig. 7). Sample SL-571 has the most unradiogenic $^{187}Os/^{188}Os$ ratio (0.1233) of the suite and falls below the estimate for depleted upper mantle (DMM) $^{187}Os/^{188}Os = 0.125–0.128$ (Snow and Reisberg, 1995; Brandon et al., 2000; Walker et al., 2002) and primitive upper mantle (PUM) $^{187}Os/^{188}Os = 0.129$ (Meisel et al., 2001).

The bulk rock $^{187}Os/^{188}Os$ ratios do not correlate with the Hf–Nd–Sr isotope compositions of clinopyroxenes (Fig. 8, Bizimis et al., 2005), nor with bulk rock 1/Os ratios. However, Os isotopes show some important correlations with major element and trace element concentrations of clinopyroxenes and the bulk rock. The samples with the most radiogenic $^{187}Os/^{188}Os$ have the highest REE (e.g. Sm, Nd), HFSE (e.g. Zr, Hf), S and Al_2O_3 contents, highest Pd/Ir ratios and lowest Mg# and Ni, Cr contents in the clinopyroxenes and the bulk rock (Fig. 9 and Fig. 5c).

5. DISCUSSION

We summarize the key observations of our geochemical study:

(1) The SLC pyroxenites show a large range in $^{187}Os/^{188}Os$ from subchondritic (only SL-571) to mostly suprachondritic ratios (0.1233–0.1643) that correlate with major element, trace element, PGE and S concentrations in the clinopyroxene and the bulk rock.

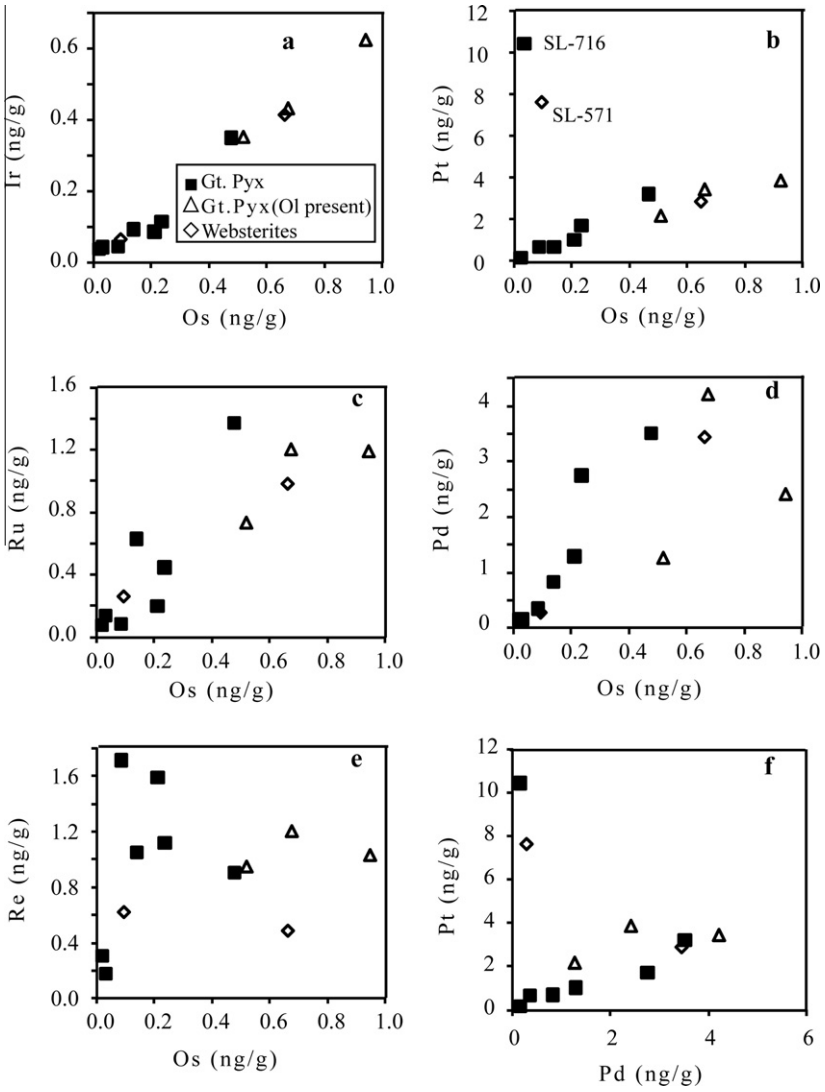

Fig. 4. Plots of Ir, Pt, Ru, Pd, and Re against Os concentrations (panels a–e) and Pt vs. Pd (panel f) in the Hawaiian pyroxenites. The samples show strong PGE intra-correlations, likely reflecting variable modal abundance of sulfides. Two samples (SL-716, and SL-571; labeled in panel b) have high Pt concentrations that do not correlate with the other PGE (panels b and f). Note that Re shows no obvious correlation with Os concentrations (panel e). Gt Pyx and Ol are abbreviations for garnet pyroxenite and olivine, respectively, and the error bars are smaller than the sample size.

(2) In contrast, the $^{187}Os/^{188}Os$ ratios do not correlate with the limited isotopic variability in Sr–Nd and Hf isotopes, and also do not show any correlations with either Re/Os or with 1/Os.

These two contrasting observations provide important constraints about the genesis of these pyroxenites and the behavior of PGE vs. lithophile elements in the oceanic lithosphere.

5.1. Origin of SLC garnet pyroxenites

The chondrite normalized PGE patterns (Fig. 3a and b) show that the pyroxenites have lower concentrations of Os and Ir relative to Pt and Pd. Experimental studies in the sulfide–silicate system (e.g. Barnes et al., 1985; Bockrath et al., 2004; Ballhaus et al., 2006) have shown that PGEs will fractionate during mantle melting in a similar fashion. In general, Os, Ir and Ru are compatible during melting and remain in the residue, while Pt, Pd and Rh are incompatible and are relatively enriched in the melt fraction (Bockrath et al., 2004; Ballhaus et al., 2006). The high Pd/Ir and Re/Os ratios (Table 2) of the pyroxenites are qualitatively similar to the patterns observed in lavas (OIB, MORB, komatiites: Bennett et al., 2000; Crocket, 2002; Peucker-Ehrenbrink et al., 2003; Puchtel et al., 2004b, 2005; Ireland et al., 2009). From this we infer that the pyroxenites originate from a melt, and are not residuals after melting. Therefore the bulk rock PGE data supports the previously proposed cumulate origin of the pyroxenites (Sen, 1983; Bizimis et al., 2005; Sen et al., 2005; Keshav et al., 2007). But whether the parental melt, and by inference the xenoliths that crystallized from

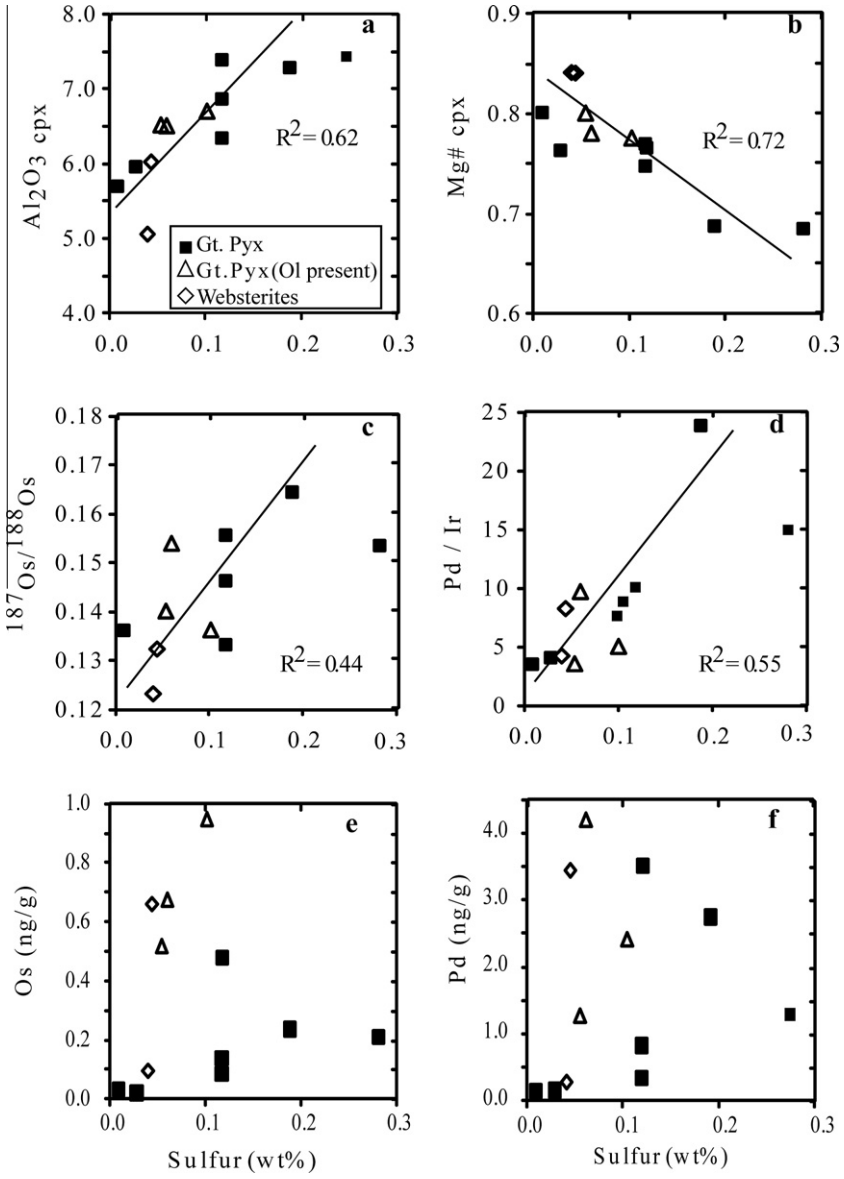

Fig. 5. Bulk rock sulfur concentrations vs. major elements in clinopyroxenes, Os isotopes, and PGE content in bulk rocks. Major element data for clinopyroxenes are from Bizimis et al. (2005). The S content shows positive correlation with Al_2O_3, Pd/Ir ratios, Os isotope systematics and negative correlations with Mg#. However, S does not show any systematic correlation with compatible (Os) or incompatible (Pd) HSE.

such melt, originate from a mid-ocean ridge (MOR) setting or the vicinity of the Hawaiian plume needs further discussion in the light of our new data.

Based on a broad correlation of Re/Os with $^{187}Os/^{188}Os$ ratios (set of five samples) Lassiter et al. (2000) proposed that the SLC pyroxenites may be tens of millions of years old. The radiogenic Os results from the ingrowth of ^{187}Os from ^{187}Re, while the pyroxenites remained stored in the Pacific lithosphere for 80–100 Myr, the approximate age of the ocean floor beneath Oahu. This amount of time is sufficient for pyroxenites to develop high $^{187}Os/^{188}Os$ ratios, but insufficient to evolve and show significant variability in the Sr–Nd–Hf compositions. If these pyroxenites are 80–100 Myr cumulates then correlations between Os isotopes and Re/Os ratios should be expected in our samples. However, no isochron relationship exists between $^{187}Os/^{188}Os$–$^{187}Re/^{188}Os$ and Fig. 7 clearly shows the lack of any significant correlations between Os isotopes and Re/Os ratios.

It was further suggested that the high Re contents of the pyroxenites (average 0.6 ng/g Lassiter et al. (2000) study, 0.9 ng/g this study) are consistent with their formation in a mid-ocean ridge setting, because MORBs have higher Re concentrations than the OIBs (average 0.926 ng/g Re_{MORB} and 0.42 ng/g Re_{OIB} (Hauri and Hart, 1997; Schiano et al., 1997; Roy-Barman et al., 1998; Ireland et al., 2009). However, the high Re concentrations in the pyroxenites may be explained by fractionation of garnet

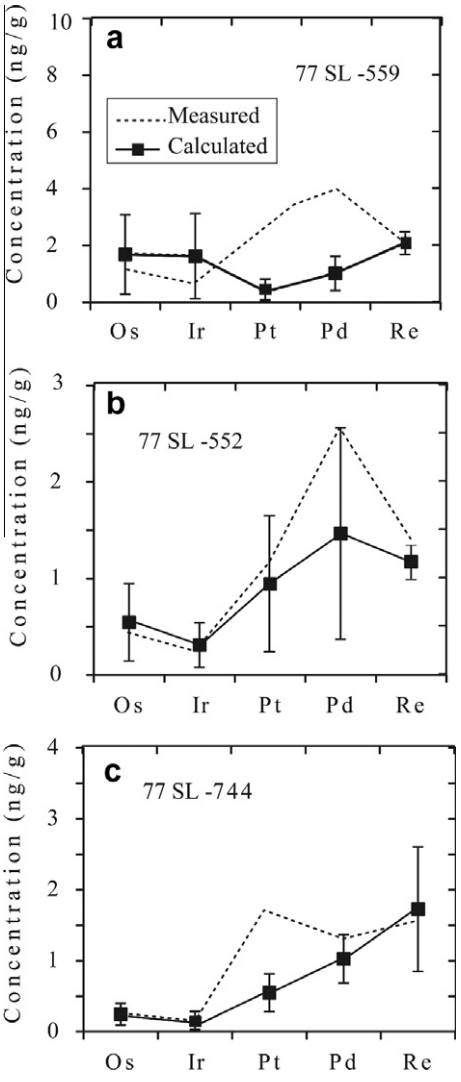

Fig. 6. (a–c) Mass balance estimates of the contribution of sulfides to the HSE budget of garnet pyroxenites. Broken lines: measured bulk rock HSE abundances; filled square: calculated HSE abundances in bulk rock, assuming no HSE in the silicates. Error bars on the calculated bulk rock data were estimated as 1σ standard deviation on the average sulfide composition (Sen et al., 2010). The measured Os and Ir values are within the range of calculated values; this suggests that sulfides are the major repository of Os and Ir in these rocks. Pt and Pd are slightly outside the range for sample number SL-744 and to a great extent in sample number SL-559, that suggests there may be smaller sulfide grains enriched in Pt and Pd (further discussed in the text). Note measured Re abundances is greater than the estimated value in SL-552.

and sulfide which are of primary magmatic origin. Sattari et al. (2002) estimated a K_D (sulfide/silicate melt) of 3.3–5.2×10^4 and Righter and Hauri (1998) estimated K_D (garnet/silicate melt) of 2.7 for Re. The K_D value obtained by Sattari et al. (2002) is almost three orders of magnitude higher than the value of <50 reported by Roy-Barman et al. (1998) and Fonseca et al. (2007). However, it should be noted that the Sattari et al. (2002) study reported the partitioning of Re between sulfide and silicates at high pressure (1 GPa) and temperature (1350 °C) conditions, in comparison to the low pressure (1 atm) experimental runs reported by Fonseca et al. (2007). When the data from the Fonseca et al. (2007) study are extrapolated to the temperature, fO_2 and fS_2 values used by Sattari et al. (2002), partition coefficient values of the order of 10^4 can be obtained. As the Hawaiian garnet pyroxenites formed at upper mantle pressure, and temperature conditions, we used the Sattari et al. (2002) study.

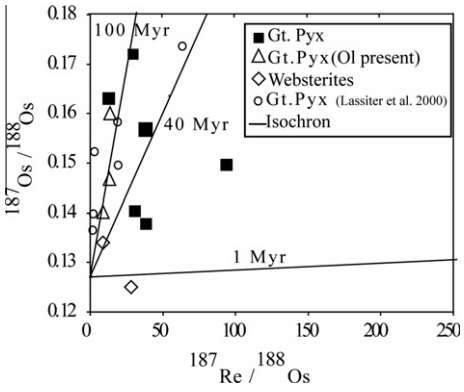

Fig. 7. Plot of $^{187}Os/^{188}Os$ vs. $^{187}Re/^{188}Os$; no isochron relationship exists in the pyroxenite xenoliths from Hawaii.

Assuming no Re in the clinopyroxene, and a bulk rock that contains 10% of garnet and 0.02% of sulfides (sample with the lowest modal abundance of sulfide, Table 1), we calculate a bulk distribution coefficient between pyroxenite and conjugate melt of $D_{Re} \sim 7$, using the partition coefficients from the Sattari et al. (2002) and Righter and Hauri (1998) studies. The Re concentrations in the pyroxenites range between 0.18 and 1.7 ng/g and assuming the $D_{Re} \sim 7$, the calculated Re concentration of a melt in equilibrium with these pyroxenites will range from 0.025 to 0.45 ng/g, which is much lower than the mean MORB Re concentration (0.926 ng/g). It is important to note that increasing the sulfide abundance ($X_{sulfide}$) in the fractionating assemblage will significantly increase the bulk D (changes in the garnet modal abundance will not cause any significant difference in our calculations), for example, if $X_{sulfide} = 0.2$ wt% the bulk D_{Re} will increase to 60. In this higher modal sulfide scenario, the melt in equilibrium with the pyroxenites will have Re concentration even lower than the above estimate. Therefore, the high Re content of the pyroxenites can be explained with sulfide and garnet fractionation from a melt similar to the Hawaiian lavas, and does not require a high Re parental melt similar to MORBs.

Fig. 3b shows that although chondrite-normalized PGE patterns of MORB and Hawaiian lavas are similar, MORB are much more depleted in PGEs than Hawaiian lavas. We calculate PGE concentrations in the parental silicate melt that would have coexisted with the pyroxenites using the following bulk distribution coefficients: $D_{Os} \sim 9$, $D_{Ir} \sim 3$, $D_{Pt} \sim 0.5$ and $D_{Pd} \sim 0.5$ (Jamais et al., 2008). The calculated parental melt compositions have an average of 38 pg/g Os, 74 pg/g Ir, 6315 pg/g Pt and 3439 pg/g Pd, whereas the average Os, Ir, Pt and Pd concentrations in Pacific MORB are 9 pg/g, 6 pg/g, 151 pg/g and 53 pg/g, respectively (Schiano et al., 1997; Tatsumi et al., 1999).

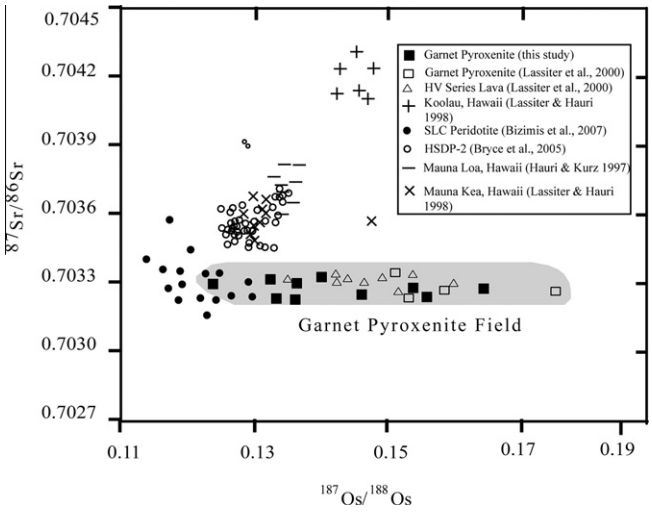

Fig. 8. $^{187}Os/^{188}Os$ vs. $^{87}Sr/^{86}Sr$ plot for the garnet pyroxenite samples from this study and Lassiter et al. (2000) study; compared with the HSDP-2 Mauna Kea lava, Mauna Loa lava, Koolau lava, HV lava and SLC peridotites. Symbol and source of the data are inside the figure. The gray area represents the garnet pyroxenite field: it shows a considerable spread across the $^{187}Os/^{188}Os$ axis and very limited spread along the $^{87}Sr/^{86}Sr$ axis.

We conclude that our PGE data for the SLC pyroxenites supports a Hawaiian plume origin, as previously proposed from the major element, trace element and Rb/Sr, Sm/Nd and Lu/Hf isotope compositions of the SLC pyroxenites (Frey, 1980; Sen et al., 1993; Bizimis et al., 2005). Although, it is reasonable to expect that mafic melts may become arrested as "veins" in the lower lithosphere during upwelling of the mantle at the MOR setting, it appears that these SLC pyroxenites are not related to the MOR setting.

5.2. Os isotope variability in the pyroxenites

As discussed earlier, the correlations of $^{187}Os/^{188}Os$ ratios with major and trace elements, PGE and S concentrations in the clinopyroxene and the bulk rock strongly suggest a primary mantle origin (Fig. 9). In the following section we investigate possible mechanisms that may explain these coupled variations.

5.2.1. Lithosphere assimilation by plume-derived melts?

A plausible scenario is that the pyroxenites represent the products of melt–peridotite reaction at the base of the lithosphere where a melt from the Hawaiian plume, enriched in incompatible elements (e.g. Fe, Al–REE–HFSE), radiogenic $^{187}Os/^{188}Os$ and $^{87}Sr/^{86}Sr$ (based on the coherent Os–Sr isotope relationship of Hawaiian lavas, Fig. 8) is assimilating the peridotitic lithosphere. Peridotites from the Pacific lithosphere have unradiogenic $^{187}Os/^{188}Os$ and $^{87}Sr/^{86}Sr$ (Bizimis et al., 2007 and Fig. 8), high abundance in compatible elements (Os, Ir, Ni and Cr), and low abundances in incompatible elements (e.g. Sr–Zr–REE). Assuming that the melt consumes peridotite, progressive reaction will result in a melt that becomes richer in Cr–Ni–Os–Ir, and poorer in REE and HFSE, while the $^{187}Os/^{188}Os$ ratio of the product melt will become increasingly unradiogenic, qualitatively consistent with the trends observed in Fig. 9. However, Lassiter et al. (2000) demonstrated that such mixing will produce highly hyperbolic mixing arrays in the $^{187}Os/^{188}Os$ vs. $^{87}Sr/^{86}Sr$ isotope space; as the plume derived melt have significantly higher Sr/Os ratio than the depleted mantle peridotite. Such mixing scenario cannot produce the variability in the Os isotopes at a nearly identical Sr isotope composition (Fig. 8).

An alternative scenario is that the plume melt is selectively assimilating peridotitic sulfides with (presumably) unradiogenic Os isotopic compositions, the assumption being that the unradiogenic Os seen in the bulk rock peridotites (Bizimis et al., 2007) is reflected in the composition of their sulfides. In this scenario, we would expect a negative correlation between sulfur contents and Os isotopes, opposite to what observed in these pyroxenites (e.g. Fig. 5c). Therefore, we consider lithospheric mantle assimilation as an unlikely process to explain the Os vs. major-trace element systematics of the SLC pyroxenites.

5.2.2. Melt mixing

The variable $^{187}Os/^{188}Os$ at near constant $^{87}Sr/^{86}Sr$ isotope ratios (similar for Nd and Hf isotopes; not shown) of the SLC pyroxenites and the rejuvenated stage lavas is in contrast with the correlated Os vs. Sr isotope compositions of the Hawaiian shield stage lavas (Fig. 8). Lassiter et al. (2000) proposed that the rejuvenated stage Hawaiian lavas and pyroxenites compositions represent melt mixing between melts from a depleted mantle source (low $^{187}Os/^{188}Os$, low $^{87}Sr/^{86}Sr$) and a young (~100 Myr) pyroxenitic mineralogy (high $^{187}Os/^{188}Os$, low $^{87}Sr/^{86}Sr$) that exists at the base of the lithosphere due to incomplete extraction of melts from the MORB melting event. It was argued that mixing of large degree melts from the pyroxenitic source and low degree melts from the peridotitic lithosphere can explain the broad negative correlation between Os isotopes and bulk rock Sr contents (and presumably other similarly incompatible elements) in the rejuvenated lavas and pyroxenites (Lassiter et al., 2000).

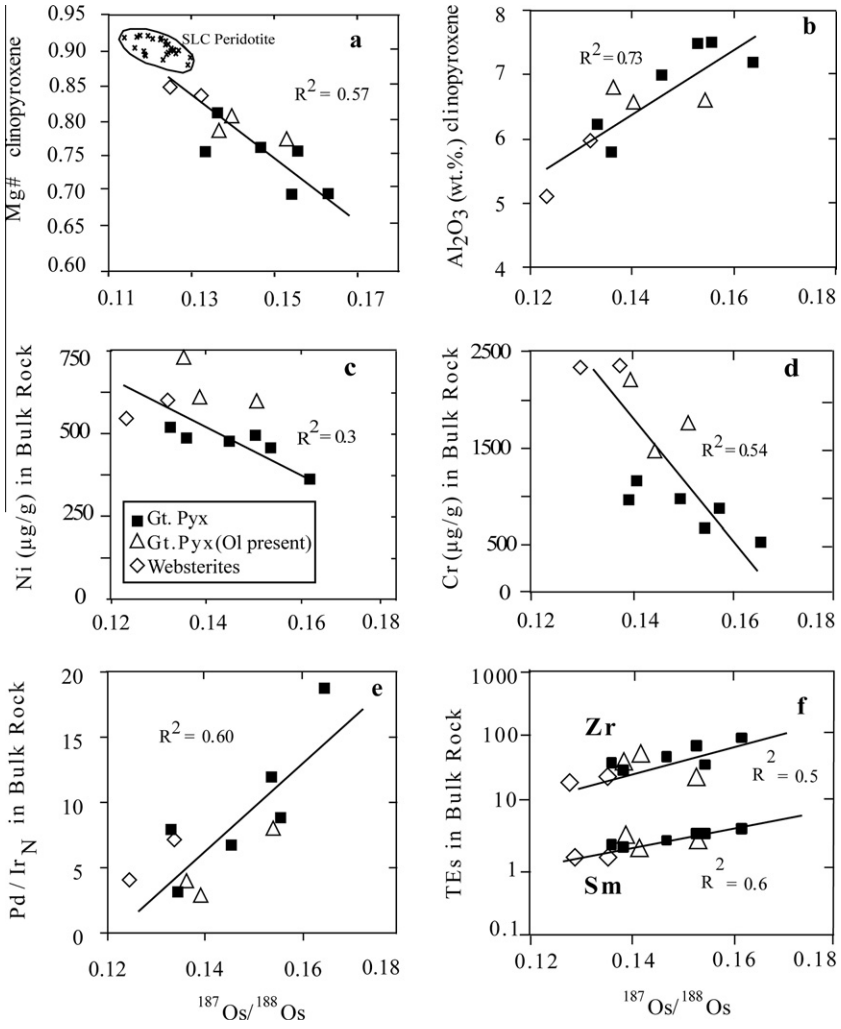

Fig. 9. Plots of $^{187}Os/^{188}Os$ ratios of the bulk rock vs. major and trace element content of clinopyroxenes and bulk rocks. Elemental data for clinopyroxenes are from Bizimis et al. (2005). Note a different *x*-axis scale in panel (a), and the log scale in panel (f). The bulk rock $^{187}Os/^{188}Os$ ratios show positive correlations with Al_2O_3, Sm, Zr and Pd/Ir and negative correlations with Mg#, Ni and Cr content of the clinopyroxenes and bulk rock. CI normalized values from McDonough and Sun (1995).

However, this model is inconsistent with our new data, as the pyroxenites with the most radiogenic Os have the highest concentrations in incompatible lithophile elements (Fig. 9). Our bulk rock pyroxenite trace element data show systematic trends between Sr, Sm and Zr (and similar trends for the other incompatible elements) and Os isotopes, and therefore high Sr contents correspond to radiogenic Os, opposite to what is inferred by Lassiter et al. (2000) study, on a fewer samples than our study. The positive correlations between Os isotopes and trace element concentrations shown here would instead require a low degree melt from an enriched source (presumably pyroxenite or eclogite) and a large degree melt from a depleted source, opposite to what is thought to occur during mantle melting based on the lower solidus of pyroxenites vs. peridotites (Hirschmann and Stolper, 1996; Keshav et al., 2004).

Yang et al. (2003) proposed an alternative model whereby melts from the plume are metasomatizing the lithospheric mantle, and generate the compositions seen in the rejuvenated stage lavas, and presumably pyroxenites. They argued that the Ba/Th, Sr/Nd, and La/Ce ratios of the rejuvenated stage lavas match the Hawaiian tholeiite compositions and not MORBs, and proposed that the variable Os isotope compositions in the HV lavas (and by inference in the SLC pyroxenites) reflect a heterogeneous depleted mantle source that is mixed with a putative Hawaiian plume melt. In that model the relatively radiogenic Sr isotope compositions of the rejuvenated volcanism relative to a MORB-like source are the result of ~2% plume melt addition to a MORB mantle. As shown in Fig. 8, the SLC pyroxenites, the HV lavas and the Hawaiian peridotites all have very similar Sr isotopic compositions ($^{87}Sr/^{86}Sr = 0.7032–7034$). If addition of 2% plume material with $^{87}Sr/^{86}Sr = 0.7036$ to a depleted mantle source with $^{87}Sr/^{86}Sr = 0.7025$ (as in the Yang et al. (2003) model) is responsible for these similar Sr isotope compositions, it is unclear how mixing of presumably different end member components at different proportions would fortuitously

produce such constant Sr isotope compositions. Furthermore, there is no obvious mechanism in this model that can generate the correlations between Os isotopes and major, trace elements we observe in the pyroxenites.

Based on the above we surmise that melt mixing between an enriched melt from either a pyroxenitic E-MORB lithology or the Hawaiian plume and the depleted lithosphere is unlikely to produce the isotope-trace element correlations and combined isotope systematics of the SLC pyroxenites. In the following we propose an alternative mechanism that can explain the observations.

5.2.3. Can fractional crystallization explain the major element systematics?

On the basis of petrography, major element, trace element chemistry and thermobarometry calculations it is well constrained that the SLC pyroxenites are not a residual product of partial melting or crystallized melts, but cumulates related to a magma fractionation process (Sen, 1988; Sen et al., 1993; Bizimis et al., 2005; Keshav et al., 2007). Here we model whether magmatic differentiation can reproduce the major element trends seen in the clinopyroxenes (Fig. 10). In order to quantitatively model such process we need an estimate of the parental melt composition. As progressive fractional crystallization will increase the concentrations of incompatible elements (i.e. Na) in the residual melt and in the successively crystallized phases, we assume that the sample with the most depleted cpx major element composition (e.g. low Na, high Mg) represents a cumulate from the most primitive parental melt available to our sampling. We used the most depleted pyroxene composition with 5.96 wt% FeO, 17.79 wt% MgO and 1.3 wt% Na_2O (sample SL-571, Bizimis et al., 2005) and calculate the major element composition of the conjugate silicate melt that would have coexisted with the clinopyroxene. We used $K_D^{\text{clinopyroxene/melt}}$ and $K_D^{\text{garnet/melt}}$ of 0.35 ± 5 and 0.45 ± 6, respectively, where K_D is the Fe–Mg exchange coefficient between crystalline and melt phase, and $D_{Na}^{\text{clinopyroxene/melt}}$ of 0.39, based on the experimental data of Walter (1998). From this parental melt composition we sequentially separated clinopyroxenes (note that garnet precipitation does not significantly effect our model calculations as garnet and clinopyroxene have very similar K_D, while Na is highly incompatible in garnet). Fig. 10 shows that with progressive fractional crystallization the resulting clinopyroxenes become increasingly Fe and Na rich (also Al, not shown) and this simple model reproduces the major element systematics of the SLC pyroxenites. This model implies that the most refractory pyroxenite (highest Mg# in cpx) may reflect the earliest fractionates and that the most Fe-rich lithologies represent the most fractionated melts.

5.2.4. Sulfide assimilation and fractional crystallization

The limited variability of Sr–Nd–Hf isotopes in the SLC pyroxenites (Bizimis et al., 2005) is also generally consistent with the above single source fractionation model, however the large variation in $^{187}Os/^{188}Os$ ratios seems to be incompatible with it. Here we propose a model where a melt that is percolating and fractionating within the Pacific lithosphere as described above is assimilating radiogenic Os

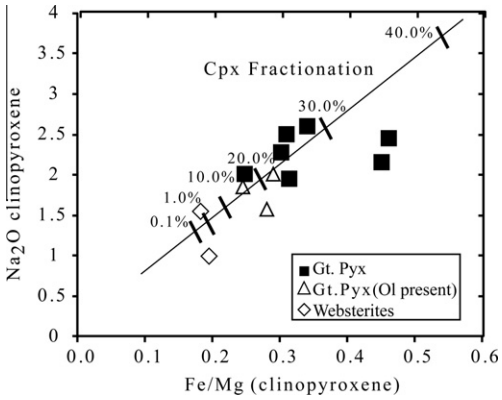

Fig. 10. Major element trends in the clinopyroxenes as a result of magmatic differentiation. The line joining the tick marks represent the chemical composition of the clinopyroxenes that are sequentially separated from the parental melt; the solid triangles represent the measured clinopyroxene composition (Bizimis et al., 2005). A single parental melt undergoing progressive silicate fractionation can produce the major element systematics of the clinopyroxenes. (Modeling description and parameters are given in Section 5.2.3.)

from grain boundary sulfide or other phases. As the melting temperature of sulfides are much lower than that of silicates (e.g. Bockrath et al., 2004; Ballhaus et al., 2006), a melt percolating through the lithosphere may preferentially melt and assimilate interstitial grain boundary sulfides. In situ Os isotope analyses of sulfides in peridotites from cratonic, abyssal and ophiolitic peridotites have shown that interstitial sulfides can have far more radiogenic Os isotopes than included sulfides, and the bulk rock (Griffin et al., 2004; Alard et al., 2005). In particular, Alard et al. (2005) showed that within a single abyssal peridotite, the interstitial sulfides of mantle origin can have $^{187}Os/^{188}Os$ ratio as high as 0.167 while the included sulfides have less radiogenic values of 0.120.

Bizimis et al. (2007) reported bulk rock Os isotope data for Hawaiian peridotites (Fig. 8), but no in situ sulfide Os isotope data is yet available. The bulk rock $^{187}Os/^{188}Os$ of the Hawaiian peridotites range from 0.114 to 0.129. As the bulk rock Os isotopic signature should be a mixture of included and interstitial sulfides it is possible that interstitial sulfides with radiogenic Os isotopes, such that recognized in the Alard et al. (2005) study also exist in the deeper oceanic lithosphere.

We envision the following process: the parental melt percolates through the lithosphere and is assimilating radiogenic Os from grain boundary phases while undergoing fractional crystallization. Here, the high Mg#, Ni and Cr-rich pyroxenites with the least radiogenic $^{187}Os/^{188}Os$ ratio represent cumulates that have undergone the least amount of fractional crystallization and a relatively less grain boundary Os assimilation, while the samples with low Mg#, Ni and Cr have undergone the largest amount of fractionation and percolation and have assimilated more radiogenic grain boundary Os.

We model this mixing scenario, where the plume derived melt is preferentially picking up grain boundary sulfides from the Pacific lithosphere. Fig. 11a shows a mixing line

between mantle derived melt and grain boundary sulfides (modeling parameters are given in the figure caption) and shows that <0.04 wt% assimilation of a sulfide (assuming 37 wt% of S in the sulfides, 0.04 wt% sulfide would require 148 μg/g of S in the lithosphere, a very reasonable estimate as the depleted mantle is thought to have 119 μg/g S; Salters and Stracke, 2004) with $^{187}Os/^{188}Os = 0.2$ can explain the range of Os isotope variability in the SLC pyroxenites. The scatter along the mixing line can be explained by sulfide precipitation due to supersaturation of sulfur in the melts either due to assimilation or fractional crystallization or both. Sen et al. (2010) have shown that the melts that crystallized the pyroxenites and the sulfides were S-saturated and here we model this sulfide precipitation processes using the Pd/Ir ratio.

As the PGE partition coefficients between sulfide/silicate are very high (e.g. >10,000; Crocket et al., 1997; Fleet et al., 1999; Sattari et al., 2002), and sulfides are the major repository of PGEs in these pyroxenites (see Section 4.3), small amount of sulfide fractionation will significantly impact the PGE concentrations of a fractionating melt, and by inference the fractional crystallized product of such melt (pyroxenites). As silicate fractionation will have negligible effects on the PGE concentrations of the residual liquid compared to sulfides, we ignore it in these calculations. We assumed a starting melt composition that would fall on the mixing line between depleted mantle derived melt and interstitial sulfides (points A, B and C in Fig. 11b). We envision that the fractional crystallization of silicates drives sulfur supersaturation in the residual melt and subsequent sulfide precipitation. We model this sulfide fractionation using sulfide/silicate partition coefficients of 20×10^3 and 60×10^3 for Pd and Ir, respectively (Crocket et al., 1997). It should be worth mentioning that the published D_{HSE} sulfide/silicate melt values show near an order of magnitude variation (Bezmen et al., 1994; Crocket et al., 1997; Roy-Barman et al., 1998; Fleet et al., 1999; Sattari et al., 2002; Fonseca et al., 2007). If we use a different set of PGE partitioning values and as long as $D_{Ir} > D_{Pd}$, the pattern would be consistent but the amount of sulfide fractionation would vary. Fig. 11b shows that limited (up to 0.1 wt%) sulfide fractionation from the sulfide assimilating melt can explain the observed range of Pd/Ir ratios in the pyroxenites, and by inference the scatter in the 1/Os and $^{187}Os/^{188}Os$ space.

The above process can explain the variation in the Os isotopes and their decoupling from the lithophile elements isotope systems (Sr, Nd, Hf) as long as the interaction between the melt and the lithospheric peridotite is isolated along the grain boundaries, which is reasonable as a basaltic melt has a lower solidus than a depleted peridotite and can effectively remain liquid within a solid peridotite. The caveat of our model is the presence of a radiogenic Os component in grain boundary phases within the lithosphere. The presence of such radiogenic components is not well understood but there is good evidence for the presence of a wide spread radiogenic mantle sulfide component in the upper mantle (Alard et al., 2005). In the Hawaiian case, the 80–100 Myr age of the lithosphere further allows for the radiogenic ingrowth of some high Re/Os sulfides that would only enhance such radiogenic signature in grain boundary sulfides. Furthermore we can speculate that as Re is more lithophile than Os, grain boundary phases other than sulfides may have extremely high Re/Os ratios (at very low Os concentrations) that will evolve quickly to extremely radiogenic Os. In situ Os isotope analyses of <10 μm size sulfides or other microscopic boundary phases are currently beyond the analytical capabilities of most instruments. At present we do not have in situ Os isotope data on sulfides from Pacific lithosphere peridotites, and the uniqueness of the proposed process needs to be attested. With the present limitation, we envision and propose that the SLC pyroxenites essentially represent crystallized melts from different stages of this reaction process at the base of the lithosphere, and that the presence of highly radiogenic grain boundary Os in the lithospheric mantle (oceanic or otherwise) can effectively decouple Os isotopes from other lithophile isotope systems.

6. RECYCLED PYROXENITES: IMPLICATION FOR THE ^{186}OS–^{187}OS OF HAWAIIAN LAVAS

Geochemistry and seismic studies suggest that the Hawaiian plume may originate at the core–mantle boundary (CMB) (Helmberger et al., 1998; Humayun et al., 2004; Montelli et al., 2004), but whether or not the Hawaiian plume is entraining materials from the outer core is a subject of debate (Brandon and Walker, 2005). The idea of core–mantle exchange came from an observation that, some Hawaiian lavas are unusually enriched in radiogenic ^{186}Os and ^{187}Os isotopes, where the coupled ^{186}Os and ^{187}Os enrichments reflect the expected high Pt/Re ratio of the outer core (Brandon et al., 1998, 1999). However, a study on the Beni Bousera massif in Morocco disputes the role of outer core and instead suggests that the coupled enrichment of ^{186}Os–^{187}Os in oceanic basalts can be explained by recycling and aging of pyroxenites plus their sulfides, as some of these may have the required high Pt/Re ratios (Luguet et al., 2008). In contrast, a recent study of pyroxenites layers in the Totalp ultramafic massif shows that those pyroxenites do not possess the requisite Pt–Re–Os composition to explain the coupled high $^{187}Os/^{188}Os$ and $^{186}Os/^{188}Os$ ratios recorded in plume-derived lavas (Van Acken et al., 2010). Our new HSE data on the SLC pyroxenites from the present day oceanic upper mantle gives us the opportunity to test the pyroxenite recycling hypothesis as a source for the coupled ^{186}Os–^{187}Os enrichments in some lavas.

Using the measured Pt/Os and Re/Os ratios of these pyroxenites we calculated the range of $^{187}Os/^{188}Os$ and $^{186}Os/^{188}Os$ compositions that these pyroxenites could develop by "ageing" them over 1, 2 and 3 Gyr from a chondritic mantle and assuming the parent/daughter ratios do not change during recycling. Fig. 12 shows the "aged" compositions of all the pyroxenites compared with the $^{186}Os/^{188}Os$–$^{187}Os/^{188}Os$ enriched Hawaiian lavas and komatiites. These pyroxenites upon aging can generate relatively radiogenic $^{187}Os/^{188}Os$ and $^{186}Os/^{188}Os$ ratios, but do not generate the steep array required by the ocean basalts (Fig. 12). Out of the 12 samples, only SL-716 and SL-571

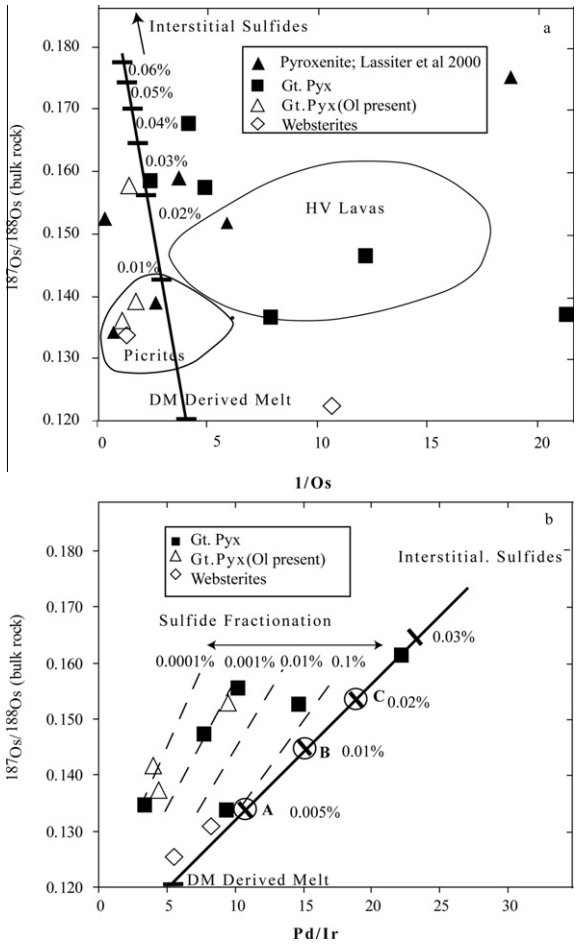

Fig. 11. Plot of 1/Os and Pd/Ir ratio vs. $^{187}Os/^{188}Os$ ratios in the bulk rock pyroxenites. The solid bold line with tick marks in both the figure represents the mixing line between depleted mantle (DM) derived melt and interstitial peridotitic sulfides. Mixing parameters are as follows: depleted mantle (DM) derived melt $^{187}Os/^{188}Os = 0.12$, Os = 250 pg/g, Ir = 200 pg/g, Pd = 1 ng/g; interstitial sulfides: $^{187}Os/^{188}Os = 0.2$, Os = 1 μg/g; Ir = 1 μg/g, Pd = 35 μg/g, similar to the PGE composition of interstitial sulfides reported by Alard et al. (2005). (a) The figure shows that the pyroxenites plot scattered along a mixing line between the DM derived melt and interstitial sulfide. (b) A (Pd = 2.75 ng/g, Ir = 0.25 ng/g), B (Pd = 4.5 ng/g, Ir = 0.3 ng/g) and C (Pd = 8 ng/g, Ir = 0.4 ng/g) represent the composition of a melt that has assimilated 0.005, 0.01 and 0.02 wt% of interstitial sulfides while percolating through the Pacific lithosphere. From A, B and C we model sulfide fractionation using the sulfide/silicate partition coefficients of 60×10^3 and 20×10^3 for Ir and Pd (Crocket et al., 1997). The dashed lines show the composition of the resulting melt after sulfide fractionation (0.0001, 0.001 wt%, etc.). Our calculations show that the range of Pd/Ir and Os isotope ratios can be explained with limited assimilation of radiogenic Os and subsequent sulfide fractionation.

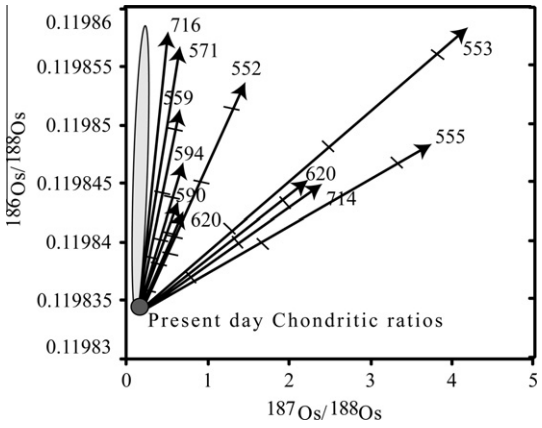

Fig. 12. Calculated present day ^{186}Os–^{187}Os isotope systematics of pyroxenites evolved 1, 2 and 3 Gyr from a chondritic earth, compared with reported high ^{186}Os–^{187}Os plume derived lavas (picritic lavas and komatiites; gray field) (Brandon et al., 1998, 1999, 2003). The pyroxenites are assumed to have chondritic $^{186}Os/^{188}Os$ and $^{187}Os/^{188}Os$ ratios at 1–2–3 Ga ago, calculated using present day $^{186}Os/^{188}Os = 0.119834$; $^{187}Os/^{188}Os = 0.127$, chondritic $^{190}Pt/^{188}Os = 0.001692$; $^{187}Re/^{188}Os = 0.40186$, and decay constants $\lambda^{190}Pt = 1.417 \times 10^{-12}$/year and $\lambda^{187}Re = 1.67 \times 10^{-11}$/year (Brandon and Walker, 2005). The pyroxenites are then evolved to present day using the $^{190}Pt/^{188}Os$ and $^{187}Re/^{188}Os$ ratios determined here (Table 2). Our calculations show that these pyroxenites will develop radiogenic ^{186}Os–^{187}Os compositions but at much shallower slope than observed in Hawaiian lavas and komatiites. This suggests that recycling of these types of mantle pyroxenites is an unlikely source for the coupled ^{186}Os–^{187}Os observed in the Hawaiian plume and elsewhere. The tick marks on the evolution trajectory represents 1–2–3 Gyr marks.

can generate a steep array in the $^{187}Os/^{188}Os$–$^{186}Os/^{188}Os$ space, however, it is not steep enough to overlap the Hawaiian lavas and komatiites field.

Brandon et al. (1999) calculated that in order to produce the steep slope of the Hawaiian picrites in $^{187}Os/^{188}Os$ vs. $^{186}Os/^{188}Os$ isotope space, their source should have a Pt/Re ratio of 88–100. The pyroxenites analyzed here have a Pt/Re range from 0.4 to 12, with only one sample with a Pt/Re ratio of 59 (Table 2). It is also important to note that none of the 23 pyroxenites reported by Van Acken et al. (2010) study have Pt/Re ratio >15 and out of the 11 samples in the Luguet et al. (2008) only one sample (GP 87T) has a high enough Pt/Re ratio (~115) to generate the required $^{187}Os/^{188}Os$ vs. $^{186}Os/^{188}Os$ enrichments in plume lavas. Therefore, it seems very unlikely that mantle pyroxenites in general may possess the required and very high Pt/Re ratio (>88) to generate, over time, the coupled enrichment of $^{187}Os/^{188}Os$ and $^{186}Os/^{188}Os$ ratios in plume derived lavas. By inference then, an outer core contribution to the Hawaiian and other komatiite plume volcanism may still be the valid hypothesis.

7. SUMMARY

The (radiogenic to unradiogenic) variability in the $^{187}Os/^{188}Os$ ratios and their correlations with PGE ratios, S, major and trace elements suggest that the $^{187}Os/^{188}Os$ signatures of the SLC pyroxenites reflect a primary magmatic process. To explain the correlations and the large variation in the $^{187}Os/^{188}Os$ ratios we propose an assimilation/fractional crystallization mechanism. In our model, major and trace element systematics of the clinopyroxenes and

bulk rock pyroxenites and the relatively constant Rb–Sr, Sm–Nd and Lu–Hf isotope systematics are best explained by fractional crystallization of a rather homogenous parental magma. We envision that during melt crystallization and percolation within the lithosphere, the parental pyroxenite melt is assimilating sulfides with radiogenic Os from the grain boundaries of the peridotitic lithosphere, without significantly reacting with the silicate portion of the lithosphere. The sulfides are preferentially mobilized during the melt–rock reaction because of their low melting temperature when compared to the melting temperature of the peridotites. The sampled pyroxenites essentially represent crystallized melts from different stages of sulfide assimilation and crystallization process at the base of the lithosphere. Our model predicts the presence of a radiogenic Os component along the grain boundaries of the peridotitic lithosphere (oceanic or cratonic). This may have significant implications for the decoupling of Os isotopes from other lithophile element isotope systems, in particular, during small degrees melting events, where grain boundaries may preferentially contribute to the melt than sulfides armored within silicates and presumably of less radiogenic Os signature. Lastly, the pyroxenites do not have the required high Pt/Re ratio to generate enriched ^{186}Os–^{187}Os isotope signature observed in some Hawaiian picrites.

ACKNOWLEDGEMENTS

We thank David Van Acken and Igor S. Puchtel for their insightful comments, all of which have improved our manuscript significantly, and Alan Brandon for editorial handling. I. Sen is thankful for the Doctoral Evidence Acquisition Fellowship award at Florida International University. Parts of this research were supported by Grants NSF-OCE: 0622827, 0852488 and 0928280 to M. Bizimis. The ICP-MS instrumentation at University of South Carolina was funded by Grant NSF-OCE 0820723. We thank Munir Humayun at Florida State University for giving advice on the PGE and Os spectrometry, and Vincent Salters for providing access to instrumentation and support. Discussions with Robert Creaser, Roberta Rudnick, Asish Basu and Rich Walker at various international meetings are greatly acknowledged. I.S. also thanks the postdoctoral scholar program at the Woods Hole Oceanographic Institution for the successful completion of the project. Sincere thanks to Rosemary Hickey-Vargas, Florentin Maurrasse, Max Tirone, Melroy Borges, Bernhard Peucker-Ehrenbrink and Jerzy Bluztajn for their comments and suggestions.

REFERENCES

Ackerman L., Walker R. J., Puchtel I. S., Pitcher L., Jelinek E. and Strnad L. (2009) Effects of melt percolation on highly siderophile elements and Os isotopes in subcontinental lithospheric mantle: a study of the upper mantle profile beneath Central Europe. *Geochim. Cosmochim. Acta* **73**(8), 2400–2414.

Alard O., Griffin W. L., Lorand J.-P., Jackson S. E. and O'Reilly S. Y. (2000) Non-chondritic distribution of the highly siderophile elements in mantle sulphides. *Nature* **407**(6806), 891–894.

Alard O., Luguet A., Griffin W. L., Lorand J. P., Gunnoun A., Burton K. W. and O'Reilly S. Y. (2005) In situ Os isotopes in abyssal peridotites bridge the isotopic gap between MORBs and their source mantle. *Nature* **436**(7053), 1005–1008.

Ballhaus C., Bockrath C., Wohlgemuth-Ueberwasser C., Laurenz V. and Berndt J. (2006) Fractionation of the noble metals by physical processes. *Contrib. Mineral. Petrol.* **152**(6), 667–684.

Barnes S. J., Naldrett A. J. and Gorton M. P. (1985) The origin of the fractionation of Platinum Group Elements in terrestrial magmas. *Chem. Geol.* **53**(3–4), 303–323.

Becker H., Horan M. F., Walker R. J., Gao S., Lorand J. P. and Rudnick R. J. (2006) Highly siderophile element composition of the Earth's primitive upper mantle: constraints from new data on peridotite massifs and xenoliths. *Geochim. Cosmochim. Acta* **70**(17), 4528–4550.

Bennett V. C., Norman M. D. and Garcia M. O. (2000) Rhenium and platinum group element abundances correlated with mantle source components in Hawaiian picrites: sulphides in the plume. *Earth Planet. Sci. Lett.* **183**(3–4), 513–526.

Bezmen N. I., Asif M., Brugmann G. E., Romanenko I. M. and Naldrett A. J. (1994) Distribution of Pd, Rh, Ru, Ir, Os and Au between sulfide and silicate metals. *Geochim. Cosmochim. Acta* **58**(4), 1251–1260.

Birck J. L., Roy-Barman M. and Capmas M. (1997) Re–Os isotopic measurements at the femtomole level in natural samples. *Geostand. Newsl.* **21**, 19–27.

Bizimis M., Griselin M., Lassiter J. C., Salters V. J. M. and Sen G. (2007) Ancient recycled mantle lithosphere in the Hawaiian plume: osmium–hafnium isotopic evidence from peridotite mantle xenoliths. *Earth Planet. Sci. Lett.* **257**(1–2), 259–273.

Bizimis M., Sen G., Salters V. J. M. and Keshav S. (2005) Hf–Nd–Sr isotope systematics of garnet pyroxenites from Salt Lake Crater, Oahu, Hawaii: evidence for a depleted component in Hawaiian volcanism. *Geochim. Cosmochim. Acta* **69**(10), 2629–2646.

Bockrath C., Ballhaus C. and Holzheid A. (2004) Fractionation of the platinum-group elements during mantle melting. *Science* **305**(5692), 1951–1953.

Brandon A. D., Norman M. D., Walker R. J. and Morgan J. W. (1999) (Super 186) Os–(super 187) Os systematics of Hawaiian picrites. *Earth Planet. Sci. Lett.* **174**(1–2), 25–42.

Brandon A. D. and Walker R. J. (2005) The debate over core–mantle interaction. *Earth Planet. Sci. Lett.* **232**(3–4), 211–225.

Brandon A. D., Walker R. J., Morgan J. W., Norman M. D. and Prichard H. M. (1998) Coupled (super 186) Os and (super 187) Os evidence for core–mantle interaction. *Science* **280**(5369), 1570–1573.

Brandon A. D., Snow J. E., Walker R. J., Morgan J. W. and Mock T. D. (2000) ^{190}Pt–^{186}Os and ^{187}Re–^{187}Os systematics of abyssal peridotites. *Earth Planet. Sci. Lett.* **177**, 319–335.

Brandon A. D., Walker I. S., Puchtel I. S., Becker H., Humayun M. and Revillion S. (2003) (Super 186) Os–(super 187) Os systematics of Gorgona Island komatiites: implications for early growth of the inner core. *Earth Planet. Sci. Lett.* **206**(3–4), 411–426.

Bryce J. G., DePaolo D. J. and Lassiter J. C. (2005) Geochemical structure of the Hawaiian plume: Sr, Nd, and Os isotopes in the 2.8 km HSDP-2 section of Mauna Kea volcano. *Geochem. Geophys. Geosyst.* **6**, Q09G18. doi:10.1029/2004GC000809.

Crocket J. H. (2002) Platinum-group elements in basalts from Maui, Hawaii: low abundances in alkali basalts. *Can. Mineral.* **40**(2), 595–610.

Crocket J. H., Fleet M. E. and Stone W. E. (1997) Implications of composition for experimental partitioning of platinum-group elements and gold between sulfide liquid and basalt melt: the significance of nickel content. *Geochim. Cosmochim. Acta* **61**(19), 4139–4149.

Fleet M. E., Crocket J. H., Liu M. and Stone W. E. (1999) Laboratory partitioning of platinum-group elements (PGE) and

gold with application to magmatic sulfide–PGE deposits. *Lithos* **47**(1–2), 127–142.

Frey F. A. (1980) The origin of pyroxenites and garnet pyroxenites from Salt Crater, Oahu, Hawaii: trace element evidence. *Am. J. Sci.* **280A**(Pt. 2), 427–449.

Fonseca R. O. C., Mallmann G., O'Neill H. St. C. and Campbell I. H. (2007) How chalcophile is rhenium? An experimental study of the solubility of Re in sulphide mattes. *Earth Planet. Sci. Lett.* **260**, 537–548.

Green D. H. (1966) The origin of the "eclogites" from Salt Lake Crater, Hawaii. *Earth Planet. Sci. Lett.* **1**(6), 414–420.

Griffin W. L., Graham S., O'Reilly S. Y. and Pearson N. J. (2004) Lithosphere evolution beneath the Kaapvaal Craton: Re–Os systematics of sulfides in mantle-derived peridotites. *Chem. Geol.* **208**(1–4), 89–118.

Hauri E. H. and Kurz M. D. (1997) Melt migration and mantle chromatography: 2. A time-series Os isotope study of Mauna Loa Volcano, Hawaii. *Earth Planet. Sci. Lett.* **153**(1–2), 21–36.

Hauri E. H. and Hart S. R. (1997) Rhenium abundances and systematics in oceanic basalts. *Chem. Geol.* **139**(1–4), 185–205.

Helmberger D. V., Wen L. and Ding X. (1998) Seismic evidence that the source of the Iceland hotspot lies at the core–mantle boundary. *Nature* **396**(6708), 251–255.

Hirschmann M. M. and Stolper E. M. (1996) A possible role for garnet pyroxenites in the origin of "garnet signature" in MORB. *Contrib. Mineral. Petrol.* **124**, 185–208.

Hu L., Humayun M. and Wittig N. (2011) Rhenium isotopic compositions of iron meteorites: initial results. *LPSC* **42**, 2487.

Humayun M., Qin L. and Norman M. D. (2004) Geochemical evidence for excess iron in the mantle beneath Hawaii. *Science* **306**(5693), 91–94.

Ireland T. J., Walker R. J. and Garcia M. O. (2009) Highly siderophile element and 187Os isotope systematics of Hawaiian picrites: implications for parental melt composition and source heterogeneity. *Chem. Geol.* **260**, 112–128.

Jackson E. D. and Wright T. L. (1970) Xenoliths in the Honolulu volcanic series, Hawaii. *J. Petrol.* **11**(2), 405–430.

Jamais M., Lassiter J. C. and Bruegmann G. (2008) PGE and Os isotopic variations in lavas from Kohala Volcano, Hawaii: constraints on PGE behavior and melt/crust interaction. *Chem. Geol.* **250**(1–4), 16–28.

Jochum K. P. and Nehring F. (Max-Plank-Institute fuer Chemie) (2006) USGS BHVO-2: GeoReM preferred values (11/2006). GeoReM. Available from: http://georem.mpch-mainz.gwdg.de.

Jochum K. P., Nehring F. and Stoll B. (Max-Plank-Institut fuer Chemie) (2006) BIR-1: GeoReM preferred values (11/2006). GeoReM. Available from: http://georem.mpch-mainz.gwdg.de.

Keshav S., Gudfinnsson G. H., Sen G. and Fei Y. (2004) High-pressure melting experiments on garnet clinopyroxenite and the alkalic to tholeiitic transition in ocean-island basalts. *Earth Planet. Sci. Lett.* **223**(3–4), 365–379.

Keshav S. and Sen G. (2001) Majoritic garnets in Hawaiian xenoliths: preliminary results. *Geophys. Res. Lett.* **28**(18), 3509–3512.

Keshav S., Sen G. and Presnall D. C. (2007) Garnet-bearing xenoliths from Salt Lake Crater, Oahu, Hawii: high-pressure fractional crystallization in the oceanic mantle. *J. Petrol.* **48**(8), 1681–1724.

Kumar N., Reisberg L. and Zindler A. (1996) A major and trace element and strontium, neodymium, and osmium isotopic study of a thick pyroxenite layer from the Beni Bousera ultramafic complex of northern Morocco. *Geochim. Cosmochim. Acta* **60**(8), 1429–1444.

Lassiter J. C. (2003) Rhenium volatility in subaerial lavas: constraints from subaerial and submarine portions of the HSDP-2 Mauna Kea drillcore. *Earth Planet. Sci. Lett.* **214**(1–2), 311–325.

Lassiter J. C. and Hauri E. H. (1998) Osmium-isotope variations in Hawaiian lavas: evidence for recycled oceanic lithosphere in the Hawaiian plume. *Earth Planet. Sci. Lett.* **164**(3–4), 483–496.

Lassiter J. C., Hauri E. H., Reiners P. W. and Garcia M. O. (2000) Generation of Hawaiian post-erosional lavas by melting of a mixed lherzolite/pyroxenite source. *Earth Planet. Sci. Lett.* **178**(3–4), 269–284.

Lorand J.-P. and Alard O. (2001) Platinum-group element abundances in the upper mantle: new constraints from in situ and whole-rock analyses of Massif Central xenoliths (France). *Geochim. Cosmochim. Acta* **65**(16), 2789–2806.

Luguet A., Pearson D. G., Nowell G. M., Dreher S. T., Coggon J. A., Spetsius Z. V. and Parman S. W. (2008) Enriched Pt–Re–Os isotope systematics in plume lavas explained by metasomatic sulfides. *Science* **319**(5862), 453–456.

Maier W. D., Barnes S.-J. and van der Merwe M. J. (2001) Platinum-group elements in the Pyroxenite Marker, Bushveld Complex: implications for the formation of the Main Zone. *S. Afr. J. Geol.* **104**(4), 301–308.

McDonough W. F. and Sun S. S. (1995) The composition of the Earth. *Chem. Geol.* **120**(3–4), 223–253.

Meisel T., Walker R. J., Irving A. J. and Lorand J.-P. (2001) Osmium isotopic compositions of mantle xenoliths: a global perspective. *Geochim. Cosmochim. Acta* **65**(8), 1311–1323.

Montelli R., Nolet G., Dahlen F. A., Masters G., Engdahl E. R. and Hung S. H. (2004) Finite-frequency tomography reveals a variety of plumes in the mantle. *Science* **303**(5656), 338–343.

Pearson D. G. and Nowell G. M. (2004) Re–Os and Lu–Hf isotope constraints on the origin and age of pyroxenites from the Beni Bousera peridotite massif: implications for mixed peridotite–pyroxenite mantle sources. *J. Petrol.* **45**(2), 439–455.

Peucker-Ehrenbrink B., Bach W., Hart S. R., Blusztajn J. S. and Abbruzzese T. (2003) Rhenium–osmium isotope systematics and platinum group element concentrations in oceanic crust from DSDP/ODP sites 504 and 417/418. *Geochem. Geophys. Geosyst.* **4**(7), 8911. doi:10.1029/2002GC000414.

Puchtel I. S., Brandon A. D. and Humayun M. (2004a) Precise Pt–Re–Os isotope systematics of the mantle from 2.7 Ga komatiites. *Earth Planet. Sci. Lett.* **224**(1–2), 157–174.

Puchtel I. S., Humayun M., Campbell A. J., Sproule R. A. and Lesher C. M. (2004b) Platinum group element geochemistry of komatiites from the Alexo and Pyke Hill areas, Ontario, Canada. *Geochim. Cosmochim. Acta* **68**(6), 1361–1383.

Puchtel I. S., Brandon A. D., Humayun M. and Walker R. J. (2005) Evidence for the early differentiation of core from Pt–Re–Os isotope systematics of 2.8 Ga komatiites. *Earth Planet. Sci. Lett.* **237**(1–2), 118–134.

Righter K. and Hauri E. H. (1998) Compatibility of rhenium in garnet during mantle melting and magma genesis. *Science* **280**, 1737–1741.

Roy-Barman M., Wasserburg G. J., Papanastassiou D. A. and Chaussidon M. (1998) Osmium isotopic compositions and Re–Os concentrations in sulfide globules from basaltic glasses. *Earth Planet. Sci. Lett.* **154**(1–4), 331–347.

Salters V. J. M. and Stracke A. (2004) Composition of the depleted mantle. *Geochem. Geophys. Geosyst.* **5**(5), Q05004. doi:10.1029/2003GC000597.

Sattari P., Brenan J. M., Horn I. and McDonough W. F. (2002) Experimental constraints on the sulfide- and chromite–silicate melt partitioning behavior of rhenium and platinum-group elements. *Econ. Geol. Bull. Soc. Econ. Geol.* **97**(2), 385–398.

Schiano P., Birck J.-L. and Allegre C. J. (1997) Osmium–strontium–neodymium–lead isotopic covariations in mid-ocean

ridge basalt glasses and the heterogeneity of the upper mantle. *Earth Planet. Sci. Lett.* **150**(3–4), 363–379.

Sen G. (1987) Xenoliths associated with the Hawaiian hot spot. In *Mantle Xenoliths* (ed. P. H. Nixon). Wiley, pp. 359–375.

Sen G. (1983) A petrologic model for the constitution of the upper mantle and crust of the Koolau Shield, Oahu, Hawaii, and Hawaiian magmatism. *Earth Planet. Sci. Lett.* **62**, 215–228.

Sen G. (1988) Petrogenesis of spinel lherzolite and pyroxenite suite xenoliths from the Koolau Shield, Oahu, Hawaii: implications for petrology of the post-eruptive lithosphere beneath Oahu. *Contrib. Mineral. Petrol.* **100**(1), 61–91.

Sen G., Frey F. A., Shimizu N. and Leeman W. P. (1993) Evolution of the lithosphere beneath Oahu, Hawaii: rare earth element abundances in mantle xenoliths. *Earth Planet. Sci. Lett.* **119**, 53–69.

Sen G., Keshav S. and Bizimis M. (2005) Hawaiian mantle xenoliths and magmas: composition and thermal character of the lithosphere. *Am. Mineral.* **90**(5–6), 871–887.

Sen I. S., Bizimis M. and Sen G. (2010) Geochemistry of sulfides in Hawaiian garnet pyroxenite xenoliths: implications for highly siderophile elements in the oceanic mantle. *Chem. Geol.* **273**, 180–192.

Snow J. E. and Reisberg L. (1995) Os isotopic systematics of altered abyssal peridotites. *Earth Planet. Sci. Lett.* **135**, 411–421.

Tatsumi Y., Oguri K. and Shimoda G. (1999) The behaviour of platinum-group elements during magmatic differentiation in Hawaiian tholeiites. *Geochem. J.* **33**(4), 237–247.

Van Acken D., Becker H., Walker R. J., McDonough W. F., Wombacher F., Ash R. D. and Piccoli P. H. (2010) Formation of pyroxenite layers in the Totalp ultramafic massif (Swiss Alps) – insights from highly siderophile elements and Os isotopes. *Geochim. Cosmochim. Acta* **74**(2), 661–683.

Völkening J., Köppe M. and Heumann K. G. (1991) Tungsten isotope ratio determinations by negative ionization mass spectrometry. *Int. J. Mass Spectrom. Ion Process.* **107**, 361–368.

Walker R. J., Prichard H. M., Ishiwatari A. and Pimentel M. (2002) The osmium isotopic composition of convecting upper mantle deduced from ophiolite chromites. *Geochim. Cosmochim. Acta* **66**(2), 329–345.

Walter M. J. (1998) Melting of garnet peridotite and the origin of komatiite and depleted lithosphere. *J. Petrol.* **39**(1), 29–60.

White R. W. (1966) Ultramafic inclusions in basaltic rocks from Hawaii. *Contrib. Mineral. Petrol.* **12**, 245–314.

Wirth R. and Rocholl A. (2003) Nanocrystalline diamond from the Earth's mantle underneath Hawaii. *Earth Planet. Sci. Lett.* **211**(3–4), 357–369.

Yang H. J., Frey F. A. and Clague D. A. (2003) Constraints on the source components of lavas forming the Hawaiian North Arch and Honolulu Volcanics. *J. Petrol.* **44**(4), 603–627.

Associate editor: Alan D. Brandon